Chloride (HCl/Cl⁻) dominates inorganic aerosol formation from ammonia in the Indo-Gangetic Plain during winter: Modeling and comparison with observations

Pooja V. Pawar[1,6], Sachin D. Ghude[1], Gaurav Govardhan[1], Prodip Acharja[1], Rachana Kulkarni[2], Rajesh Kumar[3], Baerbel Sinha[4], Vinayak Sinha[4], Chinmay Jena[5], Preeti Gunwani[1], Tapan Kumar Adhya[6], Eiko Nemitz[7], and Mark A. Sutton[7]

[1]Indian Institute of Tropical Meteorology (IITM), Ministry of Earth Sciences, Pune, India
[2]Savitribai Phule Pune University, Pune, India
[3]National Center for Atmospheric Research (NCAR), Boulder, CO, USA
[4]Department of Earth and Environmental Sciences, Indian Institute of Science Education and Research Mohali, Punjab, India
[5]India Meteorological Department (IMD), Ministry of Earth Sciences, Lodhi Road, New Delhi, India
[6]Kalinga Institute of Industrial Technology (KIIT), Bhubaneshwar, India
[7]UK Centre for Ecology & Hydrology (UKCEH), Edinburgh, UK

Correspondence to: Sachin D. Ghude (sachinghude@tropmet.res.in)

Abstract. The Winter Fog Experiment (WiFEX) was an intensive field campaign conducted at Indira Gandhi International Airport (IGIA) Delhi, India, in the Indo-Gangetic Plain (IGP) during the winter of 2017-2018. Here, we report the first comparison in South Asia of high temporal resolution simulation of ammonia (NH_3) along with ammonium (NH_4^+) and total NH_x (= NH_3 + NH_4^+) using the Weather Research and Forecasting model coupled with chemistry (WRF-Chem) and measurements made using the Monitor for AeRosols and Gases in Ambient Air (MARGA) at the WiFEX research site. In the present study, we incorporated Model for Simulating Aerosol Interactions and Chemistry (MOSAIC) aerosol scheme into the WRF-Chem. Despite simulated total NH_x values/variability often agreed well with the observations, the model frequently simulated higher NH_3 and lower NH_4^+ concentrations than the observations. Under the winter conditions of high relative humidity (RH) in Delhi, hydrogen chloride (HCl) was found to promote the increase in the particle fraction of NH_4^+ (which accounted for 49.5 % of the resolved aerosol in equivalent units) with chloride (Cl^-) (29.7 %) as the primary anion. By contrast, the absence of chloride (HCl/Cl^-) and their chemistry in the standard WRF-Chem model results in the prediction of sulfate (SO_4^{2-}) as the dominant inorganic aerosol anion. To understand the mismatch associated with the fraction of NH_x in the particulate phase (NH_4^+/NH_x), we added HCl/Cl^- to the model and evaluated the influence of its chemistry by conducting three sensitivity experiments using the model: No HCl, Base Case HCl (using a published waste burning inventory), and 3×Base HCl run. We found that 3×Base HCl increased the simulated average NH_4^+ by 13.1 µg m⁻³ and NH_x by 9.8 µg m⁻³ concentration while reducing the average NH_3 by 3.2 µg m⁻³, which is more in accord with the measurements. Thus HCl/Cl^- chemistry in the model increases total NH_x concentration, which was further demonstrated by reducing NH_3 emissions by a factor of 3 (-3×NH_3_EMI) in the 3×Base HCl simulation. Reducing NH_3 emissions in the 3×Base HCl simulation successfully addressed the discrepancy between measured and modeled total NH_x. We conclude that modeling the fate of NH_3 in Delhi requires a correct chemistry mechanism accounting for chloride dynamics with accurate inventories of both NH_3 and HCl emissions.

1 Introduction

The Indo-Gangetic Plain (IGP) is one of the global hotspots of atmospheric ammonia (NH_3) and faces a range of environmental challenges, particularly during the winter season, including adverse air pollution episodes, especially as NH_3 plays a substantial role in secondary aerosol formation (Ghude et al., 2020, 2008b, 2008a; Kumar et al., 2021; Saraswati et al., 2019; Sharma et al., 2020; Singh et al., 2021). Atmospheric NH_3, along with oxides of nitrogen (NO_x), together account for the largest source of reactive nitrogen (N_r), which is primarily emitted by agricultural activities, livestock population, industrial activities, and transportation (Ghude et al., 2009, 2010, 2012, 2013; Móring et al., 2021; Pawar et al., 2021; Sutton et al., 2017b). Ammonia in the environment plays a crucial role in atmospheric chemistry and the eutrophication and acidification of ecosystems (Datta et al., 2012; Mandal et al., 2013; Pawar et al., 2021; Sharma et al., 2008, 2012, 2014b). Control of NH_3 becomes a key priority in an emerging international strategy to manage the global nitrogen cycle (Gu et al., 2021; Sutton et al., 2020). Ammonia is one of the important aerosol precursor gases, and ammonium (NH_4^+) is a major counter ion for the three anions such as chloride (Cl^-), nitrate (NO_3^-), and sulfate (SO_4^{2-}) contributing to $PM_{2.5}$ composition (Seinfeld et al., 2016). In addition, as the dominant alkaline gas in the atmosphere, NH_3 has attracted the interest of scientific researchers since it has been known to promote new aerosol formation both in the initial homogeneous nucleation and in the subsequent growth, especially during wintertime (Acharja et al., 2020, 2021; Ali et al., 2019; Duan et al., 2021; Wagh et al., 2021).

In this study, we focus on wintertime since this season is characterized by low-to-dense fog events, lower temperature (T), and variability of relative humidity (RH), which fluctuates from 40 to 100 % (Ghude et al., 2017; Kumar et al., 2020). Ammonia acts as a neutralization agent for determining the acidity of aerosol particles (Acharja et al., 2020; Ali et al., 2019; Ghude et al., 2017). It also affects $PM_{2.5}$, the acidity of clouds, and the wet deposition of nitrogen by neutralizing acidic species (Gu et al., 2021; Xu et al., 2020). Increasing NH_3 concentration over Delhi compared with the surrounding area leads to an increase in $PM_{2.5}$ concentrations (Ghude et al., 2022; Sharma et al., 2008, 2012, 2014a), which in turn affects air quality, human health, and climate (Behera et al., 2013; Ghude, 2016; Ghude et al., 2008b; Nivdange et al., 2022; Sutton et al., 2017a; Sutton and Howard, 2018).

Satellite observations (Van Damme et al., 2018; Warner et al., 2017), chemical transport models (CTMs) (Clarisse et al., 2009, 2010; Wang et al., 2020b), and ground-based observations (Pawar et al., 2021) revealed that the IGP is the largest regional hotspot of NH_3 concentrations on Earth. Previous studies have identified various sources of NH_3, for example, agricultural activities, industrial sectors, motor vehicles, garbage, sewage, and urine from rural populations at the global scale (Behera et al., 2013; Huang et al., 2012; Sutton et al., 2008). However, in Delhi, agricultural activity (including surrounding arable and sub-urban livestock farming) is estimated to be the dominant source of NH_3, along with traffic emissions (Kuttippurath et al., 2020; Móring et al., 2021; Sharma et al., 2020), but its emissions are subject to large uncertainty. Globally, various modeling efforts have investigated the relative effectiveness of reducing NH_3 emissions in curtailing $PM_{2.5}$ formation (Gu et al., 2021; Pinder et al., 2007, 2008; Zhang et al., 2020). However, over India, the impact on reducing $PM_{2.5}$ might be limited because NH_3 emission reductions may be more challenging due to its diverse and area-wide sources. Ianniello et al. (2010) and Lan et al. (2021) have investigated the variation of atmospheric NH_3 at an urban and suburban site of Beijing with respect to meteorological factors, where RH was found to be a strong factor in influencing the NH_3 mixing ratio. A few studies over Asia have highlighted the gas-to-particle conversion of NH_3 in Delhi (Acharja et al.,

79   2021; Saraswati et al., 2019) and China and its subsequent impact on the aerosol formation (Wang et al., 2015;

80   Xu et al., 2020). Furthermore, excess NH_3 during fog can also enhance secondary aerosol formation in Delhi

81   during winter (Acharja et al., 2021). However, the wintertime behavior of NH_3 in Delhi in CTMs has not yet been

82   investigated and remains poorly understood (Ellis et al., 2011; Metzger et al., 2006). In a recent study, Pawar et

83   al. (2021) highlighted uncertainties associated with gas-to-particle partitioning of NH_3 in a global model

84   MOZART-4 and found a significant overestimation of NH_3 in the model compared with the measurements. The

85   overestimation of NH_3 in the model led the authors to hypothesize that a source specific NH_3 emission inventory

86   in India, considering agricultural statistics on fertilizer use and animal distribution, was missing. Also, there was

87   a need for a high-resolution regional model with advanced chemistry to resolve the NH_3 emissions on the local

88   scale.

89   The present study utilizes the regional Weather Research and Forecasting model coupled with chemistry

90   (WRF-Chem) interpreted using measurements from the Winter fog Experiment (WiFEX), including NH_3, water-

91   soluble ions in $PM_{2.5}$, other trace gases, and meteorological parameters during December-January, 2017-18. For

92   the first time in South Asia, we discuss and compare the modeled and observed temporal variation in gaseous

93   NH_3, particulate NH_4^+, and total NH_x (= $NH_3 + NH_4^+$). Since we found that the total modeled NH_x matches well

94   with the observations, we investigate the ability of the model to accurately describe the gas-to-particle partitioning

95   of the measurements (MARGA) by evaluating the fraction of NH_x in the particulate phase (NH_4^+/NH_x). We

96   conducted several sensitivity experiments with and without adding anthropogenic waste burning emissions of

97   hydrochloric acid (HCl) in the model. The updated model with HCl/Cl^- chemistry was used to analyze and

98   compare the temporal variation of NH_3, NH_4^+, and total NH_x from the WiFEX measurements.

99   **2. Data and methodology**

100   **2.1 Observational datasets**

101   **2.1.1 Description of MARGA**

102   In the present study, we used the same dataset which was previously published by Acharja et al. (2020)

103   and 2021), which described the aerosol time-series and chemistry measured with a Monitor for AeRosols and

104   Gases in Ambient Air-model 2S instrument (MARGA). The MARGA system has two channels, one for sampling

105   PM_1 and the other for sampling $PM_{2.5}$ for ground-based observations. The MARGA (two sampling boxes,

106   analytical box, and connected pumps) was located inside the Indira Gandhi International Airport (IGIA), New

107   Delhi (28.56° N, 77.09° E), with the inlet PM_1 and $PM_{2.5}$ impactors fixed on the terrace with 2 m long inlet lines

108   sampling outdoor air at 8 m above ground and 2 m above the rooftop. Measurements covered a winter period (19

109   December 2017 to 21 January 2018) with frequent moderate to dense fog events. Following intake through the

110   PM_1 and $PM_{2.5}$ impactors, the air was passed through two parallel inlet tubes 2 m long and 14 mm inner diameter

111   PolyTetraFluoroEthylene (PTFE) to the PM_1 and $PM_{2.5}$ sampling channels of the MARGA. The air flow rate in

112   each MARGA sampling box is regulated to a volumetric flow of 1 m^3 h^{-1}. The measurements are close to real-

113   time, as two sets of syringes are employed to collect the samples in which a set of syringes collects the sample

114   and another set sends the collected samples from the previous hour for analysis. Each MARGA sampling system

115   consists of a steam jet aerosol collector (SJAC) and a wet rotating denuder (WRD) for collecting and measuring

116 water-soluble inorganic particulate species and gases in the ambient air. The continuous coating of the WRD by
117 a thin film of absorption solution (10 ppm hydrogen peroxide (H_2O_2)) allows the diffusion of gases into the
118 absorption solution. By contrast, the low diffusion velocity of sub-micron particles restricts the ability of water-
119 soluble aerosols to diffuse into the absorption solution. The absorption solution is continually changed to replace
120 that abstracted for ion chromatography (IC) analysis of the dissolved gases. The air stream, depleted of gases by
121 the WRD, subsequently enters the SJAC, where the steam enhances water-soluble aerosols to grow, allowing their
122 mechanical capture in a cyclone. The aqueous solutions deriving from two cyclones (for PM_1 and $PM_{2.5}$,
123 respectively) are then supplied to the IC for chemical analysis (Acharja et al., 2020).

124   Ambient surface concentrations of NH_3 along with other trace gases (HCl, nitrous acid (HONO), nitric
125 acid (HNO_3), and sulfur dioxide (SO_2) and water-soluble inorganic components of PM_1 and $PM_{2.5}$ (Cl^-, nitrate
126 (NO_3^-), SO_4^{2-}, NH_4^+, sodium (Na^+), potassium (K^+), magnesium (Mg^{2+}), and calcium (Ca^{2+}) were then quantified
127 online by anion and cation chromatography in the analytical box at an hourly resolution. We have used only $PM_{2.5}$
128 inorganic water-soluble components and the gaseous measurements (available from both the PM_1 and $PM_{2.5}$
129 MARGA collection systems). Since NH_4^+ with the three major anions: Cl^-, NO_3^- and SO_4^{2-} constituted 97.3 %
130 of the total measured ions in $PM_{2.5}$ (Acharja et al., 2020), we consider these four significant ions in our present
131 study. In contrast, the remaining ionic species (i.e., Na^+, K^+, Mg^{2+}, and Ca^{2+}) contributed only about 3 % of the
132 total measured ions and were neglected as it would not impact our present study significantly (Acharja et al.,
133 2020). Anions are separated in a Metrosep A Supp-10 (75/4.0) column with sodium carbonate (Na_2CO_3) and
134 sodium bi-carbonate ($NaHCO_3$) (7/8 mmol l^{-1}) eluent. Whereas for cations separation, a Metrosep C4 (100/4.0)
135 cation column with 3.2 mmol l^{-1} HNO_3 eluent was used (Acharja et al., 2020). To suppress the eluent background
136 conditivity of anion chromatographs, three ion exchange units were used to ensure that the ion exchange unit is
137 regenerated in each analysis. 1 M Phosphoric acid (H_3PO_4) was used for this purpose. This was performed to
138 improve the signal-to-noise (S/N) of the anion chromatographs. Details of the MARGA instrument can be found
139 in Makkonen et al. (2012), Thomas et al. (2009), Twigg et al. (2015).

2.1.2 Quality assurance/quality control (QA/QC) of MARGA

141 To ensure the observation's accuracy and check the data's quality, we have followed best practices during the
142 study. The eluents, absorption, and regenerant solutions were prepared with minimum manual intervention. The
143 operational parameters like anion and cation conductivity, SJAC heater temperature, column oven temperature,
144 and airflow were regularly monitored to keep them within the safe limit. In addition to these, before injection of
145 each sample into the anion and cation IC columns, the Lithium Bromide (LiBr) internal standard solution
146 containing 320 µg l^{-1} lithium (Li^+) and 3680 µg l^{-1} bromide (Br^-) was mixed with each sample to provide
147 calibration of each analysis. This ensures that each analysis is calibrated, and the concentration of gaseous and
148 ionic samples are measured accurately. The PM_1 and $PM_{2.5}$ impactors were typically cleaned fortnightly to remove
149 any material that may have stuck on the surface and inlets of the impactors. The lower detection limits (LODs) of
150 the species monitored by MARGA were mentioned in Acharja et al. (2021). It shows that concentrations of species
151 like Cl^-, NO_3^-, SO_4^{2-}, NH_4^+, SO_2, and NH_3 were always higher than LODs during the winter period. But,
152 concentrations of species like Na^+, K^+, Ca^{2+}, Mg^{2+}, HCl, HONO, and HNO_3 were sometimes below LODs, but
153 the fraction of it was less than ~10 % of the total observation period. We have omitted these values and treated
154 them as NA. As the fraction of observational hours is less and these species contribute much less to the PM_1 and

155 PM$_{2.5}$ mass concentrations, we believe below LODs values would not significantly deviate our results. The quality

156 of the data obtained was then checked using the ion-balance method. As an additional quality check, the ratio of

157 the sum of cations to anions (neq m^{-3}) was used as an indicator for the viable data. We have checked the cation-

158 to-anion ratio of each hourly sample expressed in the unit of neq m^{-3}. We accepted only those values near to unity

159 and rejected those not within the 10 % error bar limit. Based on this evaluation method, overall, for the campaign,

160 the ratio was near unity (1.06 for PM$_1$ and 0.96 for PM$_{2.5}$). Excellent charge balance between anions and cations

161 measured by the system also confirms that there are no significant contamination issues associated with the aerosol

162 measurements. Values in slight excess of unity may indicate the presence of formate and acetate in the aerosol,

163 which MARGA does not measure. Further detail on the quality control of MARGA can be found in Acharja et al.

164 (2020).

2.1.3 Other ground-based measurements

166 Hourly NO$_x$ measurements were made by the chemiluminescence method, and hourly ozone (O$_3$) measurements

167 were made by the UV photometric method (CPCB, 2011) at the nearest air quality monitoring station (AQMS) of

168 IGIA operated by the Central Pollution Control Board (CPCB). CPCB follows the United States Environmental

169 Protection Agency (USEPA) approved AC32M NO$_x$ and 42M O$_3$ analyzer manufactured by Environment S. A.

170 India Private Limited. We used one-hour monitored NO$_x$ and O$_3$ values in our study. These air quality monitoring

171 stations' quality control and assurance processes were followed as outlined in CPCB (2014, 2020). For data quality

172 of CPCB, we omitted all those observed values which fell below LOD of the instrument (2 µg m^{-3} for NO$_x$ and 4

173 µg m^{-3} for O$_3$) (Technical specifications for CAAQM station, 2019) and above 500 µg m^{-3} for NO$_x$ and 140 µg m^{-3}

174 for O$_3$ and treated them as NA at a given site. For the NO$_x$ and O$_3$ datasets, only a small fraction of data (2 %)

175 were outside the instrument operating ranges specified. This step aims to remove any short-term local influence

176 that the models cannot capture and retain the regional-scale variability because the nearest sites are located in the

177 urban environment. We removed a single spike represented by a change of more than 100 µg m^{-3} in just 1 hour

178 (h) for all the data in CPCB monitoring stations to filter out random fluctuations in the observations. We removed

179 some very high NO$_x$ and O$_3$ values that appeared in the time series right after measurement gaps. Meteorological

180 parameters, including air temperature (T), relative humidity (RH), wind speed, and wind direction, were measured

181 with the automatic weather station (AWS) platform on a 20 m flux tower (Ghude et al., 2017). For detailed

182 information on the measurement site and its meteorological parameters, refer to (Ali et al., 2019).

2.2 WRF-Chem v 3.9.1 model

184 The Weather Research and Forecasting model coupled with chemistry (WRF-Chem v3.9.1) was employed in this

185 study to simulate atmospheric gases and aerosols over Delhi during the peak winter period, starting from 19

186 December 2017 to 21 January 2018. We recently used a similar model configuration to simulate the air quality

187 over Delhi (Ghude et al., 2020; Kulkarni et al., 2020). This study used the Model for Ozone And Related chemical

188 Tracers (MOZART-4) gas-phase chemical mechanism coupled with the Model for Simulating Aerosol

189 Interactions and Chemistry (MOSAIC) aerosol scheme, that simulates SO$_4^{2-}$, NH$_4^+$, NO$_3^-$, methanesulfonate, Na$^+$,

190 Ca^{2+}, Cl$^-$, carbonate, black carbon, and primary organic mass. Other inert minerals, trace elements, and inorganic

191 species are lumped together as different inorganic masses. MOSAIC allows gas-to-particle formation, which

192 includes NH$_3$, HCl, sulfuric acid (H$_2$SO$_4$), HNO$_3$, and methane sulfonic acid (MSA), and also includes secondary

193   organic aerosols (SOA). Aerosol size distributions are represented by a sectional aerosol bin approach with four

194   size bins (Georgiou et al., 2018). MOSAIC incorporates the thermodynamic and gas-particle partitioning module

195   described by Zaveri et al. (2008). To reduce the computational cost, we selected a 4-bin MOSAIC mechanism

196   that simulates thermodynamic equilibrium and other aerosol processes such as condensation, coagulation, and

197   nucleation. The same mechanism has been widely used with WRF-Chem for simulations outside India (Bucaram

198   and Bowman, 2021; Sha et al., 2019; Yang et al., 2018), but only a limited number of studies have applied it to

199   the Indian domain to include more detailed chemistry and species (Gupta and Mohan, 2015; Jena et al., 2020;

200   Kumar et al., 2018). The SOA formation in MOSAIC is simulated using the volatility basis set approach (Knote

201   et al., 2015). For consistency with the $PM_{2.5}$ MARGA measurements, we have chosen 3-bins according to

202   simulated aerosols size (0.04–0.156 μm; 0.156–0.625 μm; 0.625–2.5 μm) in accordance with the WRF-Chem

203   aerosol size distribution.

204   The model domain covers the entire northern region of India, but here model simulations are compared

205   with the observations at IGIA, New Delhi (28.56° N, 77.09° E). The domain was set with a horizontal grid-spacing

206   of 10 km in both the latitudinal and longitudinal directions. The model top vertical grid included 47 vertical levels,

207   with the model top set to 10 hPa. The physical parameterization schemes of model configuration are the same as

208   those described by Ghude et al. (2020) and Jena et al. (2021). EDGAR-HTAP (Emission Database for Global

209   Atmospheric Research for Hemispheric Transport of Air Pollution) for the year 2010 at 0.1° x 0.1° grid resolution

210   was used in this study for anthropogenic emissions of aerosols and trace gases ($PM_{2.5}$, PM_{10}, OC, BC, CO, NO_x,

211   etc.) and are scaled to 2018 as per Jena et al. (2021). Biogenic emissions are calculated online using the Model of

212   Emissions of Gases and Aerosols from Nature version 2.1 (MEGAN2.1) (Guenther et al., 2006), and dust

213   emissions are based on the traditional Goddard Global Ozone Chemistry Aerosol Radiation and Transport

214   (GOCART) dust scheme that works with MOSAIC (Ginoux et al., 2001). Fire INventory from NCAR (FINNv1.5)

215   was used in this study for daily open biomass burning emissions that are vertically distributed within the model

216   using Freitas et al. (2007). The chemical initial and lateral boundary conditions come from the global model

217   simulations from the Model for Ozone and Related Chemical Tracers (MOZART-4), and the meteorological initial

218   and lateral boundary conditions are provided from the fifth generation European Centre for Medium-Range

219   Weather Forecasts (ECMWF) atmospheric reanalysis of the global climate (ERA5) with six-hourly temporal

220   resolution. The simulations were reinitialized every fifth day to limit the growth of meteorological errors in our

221   simulations, but the chemical fields were carried forward from the previous simulation.

222   **3. Results and Discussion**

223   **3.1 Comparison of temporal variation in NH_3, NH_4^+, and total NH_x using WRF-Chem and MARGA**

224   **3.1.1 Diurnal variation**

225   To investigate how well a state-of-the-art chemical transport model performs in capturing the diurnal behavior of

226   NH_3 and NH_4^+, we compared observed and model-simulated diurnal profiles of NH_3 and NH_4^+. Figure 1 displays

227   the comparison of diurnal variation (00:00 to 23:00 Indian Standard Time (IST)) in meteorological parameters (T

228   and RH) at the IGIA site in Delhi (Fig. 1a) along with NH_3 and NH_4^+ averaged over the study period (Fig. 1b)

229   between observations and model. We adopted diurnal variation in emissions from a recent study by Jena et al.

230 (2021). Note that diurnal variability in the model simulations is primarily controlled by the planetary boundary
231 layer mixing. We first investigated the ability of WRF-Chem to accurately predict the meteorological parameters
232 of RH and T, which are important determinants of the gas-to-aerosol partitioning of (semi-) volatile compounds.
233 As shown in Fig. 1a, simulated T and RH are in reasonable agreement with the observations, with the simulated
234 RH values falling in the range of 50–90 %. Overall, it can be seen that the model shows cold and wet bias compared
235 to the observations but shows warm bias (about 2-3 ℃) and dry bias (about 10-12 %) in the afternoon hours. In
236 spite of the small change in the amplitude of the diurnal cycle of RH, the phase characteristics of the diurnal cycle
237 of both T and RH are reasonably well captured by the model. Figure 1b shows that simulated NH_3 and NH_4^+ are
238 very different compared with the MARGA measurements. The model predicts an average NH_3 and $NH_4^+ \pm 1\sigma$
239 mass loading of 56.7 ± 14.3 and 14.7 ± 4.9 µg m^{-3}, respectively, while MARGA measurements indicate an average
240 NH_3 and $NH_4^+ \pm 1\sigma$ mass loading of 28.2 ± 12.4 and 36.9 ± 15.1 µg m^{-3}, respectively. We find the diurnal variation
241 of gas-phase NH_3 is significantly overestimated by the model (Normalised Mean Bias (NMB) = 1.02). On the
242 contrary, NH_4^+ is underestimated by about 60 % (NMB = -0.60). Simulated NH_3 concentrations peak between
243 07:00-09:00 and 22:00-23:00 h with bimodal variation, whilst MARGA shows a single peak around 12:00-13:00
244 h. On the contrary, a nearly flat diurnal profile of NH_4^+ is predicted by the model, whereas the average MARGA
245 NH_4^+ concentration maxima and minima were observed during night-time (16:00-03:00 h) and daytime (03:00-
246 08:00 and 09:00-16:00 h), respectively.

247   We also looked into the average diurnal profile of NO_x and NH_3 during dense fog events, and the details
248 can be found in the supplement (Fig. S1 and S2 in the Supplement). It is evident that the observed daytime peak
249 of NH_3 did not coincide with NO_x peaks, suggesting that traffic emissions do not contribute significantly to the
250 observed NH_3 rise. The observed correlation between fog water and enhanced NH_3 pulses is consistent with what
251 would also be expected from the evaporation of dew (Sutton et al., 1998; Wentworth et al., 2014, 2016) (S2 in the
252 Supplement) but is not sufficient to identify whether it is the main cause of the daytime increase of NH_3. In the
253 future, measurements of the dew water NH_4^+ and the accumulation of dew water would be ideal for illuminating
254 the contributing processes. The daytime increase in NH_3 concentration could be associated with NH_4^+ aerosol
255 volatilization driven by an associated sharp change in T and RH (~ 11:00-12:00 h) (Sutton et al., 2009a, 2013)
256 off-ground surfaces. The fastest increase in T is 12:00 h, which is indeed when NH_3 was at maximum
257 concentration indicating gas-to-particle partitioning may impact the diurnal behavior of NH_3 at Delhi during
258 winter (Sutton et al., 2009a, 2009b). However, in the model, because the largest increase in simulated NH_3 also
259 precedes the large changes in simulated meteorological parameters, and because the simulated particulate NH_4^+
260 is flat compared to observations, simulated meteorology is ruled out as a significant contribution to high bias in
261 simulated NH_3. Also, the current model does not include the bidirectional exchange of NH_3 with surfaces such as
262 dew and fog water.

263 **3.1.2 Daily mean variation**

264   To assess the validity of the model, the ratio between simulated and observed (model/obs) was tested.
265 Figure 2 displays the model/obs ratio of daily mean variations in the NH_3, NH_4^+, and total NH_x concentrations.
266 The model shows large differences in NH_3 and NH_4^+ compared with observations. We find a model/obs higher
267 than 1 (1.5-4.5) in simulated NH_3, indicating the model is biased high (NMB = 1.02), while there is a poor
268 agreement for NH_4^+ (model/obs less than 0.5), indicating model is biased low (NMB = -0.62). There is good

269   agreement between the modeled total NH_x, which is mostly consistent with the observation (model/obs close to

270   1) with a small bias (NMB = 0.08). Despite the adequate ability of the model to reproduce the accurate total NH_x,

271   the model is biased low for NH_4^+ and high for NH_3, indicating that the model's representation of the gas-to-particle

272   partitioning is not correct. It is, therefore, necessary to understand missing chemical processes in gas-to-particle

273   partitioning responsible for the overestimation of NH_3 and underestimation of NH_4^+ in the model.

274   **3.2 Gas-to-particle partitioning**

275   We investigated the ability of the model to accurately describe the gas-to-particle partitioning of the measurements

276   (MARGA) by evaluating the fraction of total NH_x in the particulate phase (NH_4^+/NH_x) (Ellis et al., 2011; Wang

277   et al., 2015) for which statistical values are summarized in Table 1. The correlation coefficient (r) indicates an

278   inverse relationship of NH_4^+/NH_x with NH_3 for both MARGA and model (r = -0.57, -0.58, respectively). A strong

279   correlation of the MARGA ratio NH_4^+/NH_x with the dominant anion concentration (Cl^-: r = 0.79) was observed.

280   However, the measurement shows a poor relationship between SO_4^{2-} and NH_4^+/NH_x followed by NO_3^-, which is

281   probably due to very low concentrations that do not change NH_4^+/NH_x significantly even when SO_4^{2-} and NO_3^-

282   are neutralized (see Fig. 6). By contrast, the model shows a strong correlation between NH_4^+/NH_x with SO_4^{2-}

283   concentration (r = 0.77). MARGA indicates high particulate fractions of NH_4^+ and Cl^- while the modeled

284   composition is dominated by NH_4^+ and SO_4^{2-}. This mismatch is due to the complete absence of Cl^- chemistry in

285   the standard model. The measured NH_4^+/NH_x suggests that anthropogenic HCl may be promoting this increase in

286   particle fraction of NH_4^+ and Cl^- via partitioning into the aerosol, deprotonating in the aerosol water, followed by

287   NH_3 partitioning and being protonated by the ionization of the strong electrolyte HCl (Chen et al., 2022; Gunthe

288   et al., 2021).

289   Figure 3 shows the percentage contribution of gases (NH_3, SO_2, HCl, HNO_3, and HONO) and $PM_{2.5}$

290   aerosol (NH_4^+, SO_4^{2-}, NO_3^- and Cl^-) during the WiFEX measurements. The pie charts for the gases show that NH_3

291   (accounting for 53.3 % of the measured total gas concentration) dominates the gas phase, followed by sulfur

292   dioxide (SO_2) (35.61 %), whereas $PM_{2.5}$ aerosol show NH_4^+ (49.5 %) as a major cation and Cl^- (29.7 %) as a

293   significant anion followed by NO_3^- (11.7 %) and SO_4^{2-} (9 %). There is also a very high amount of SO_2 reaching

294   the site from the nearby industrial area, which is not converted to SO_4^{2-} very quickly (Acharja et al., 2021). In a

295   normally NH_3-rich atmosphere, gas-phase oxidation of SO_2 is much slower than the aqueous phase oxidation by

296   O_3, and due to nearby sources, much of the sulfur is present as SO_2 (Li et al., 2007). This appears to be because

297   of the slow rate of gas phase oxidation of SO_2. Although the atmosphere is rich in NH_3, in principle favoring

298   aqueous phase oxidation via O_3, it appears that O_3 concentrations are often insufficient (mean = 36.3, median =

299   33.8, minimum = 26.5, and maximum = 53.9, ug m^{-3} respectively) at the IGIA site (Fig. S3 in the Supplement).

300   Hence for many periods during the WIFEX campaign, SO_4^2 and NO_3^- are very low, with the result that the

301   NH_4^+/NH_x ratio does not change appreciably when SO_4^{2-} is neutralized (Table 1).

302   According to thermodynamic equilibrium theory, an aqueous solution maintains charge neutralization

303   initially by balancing NH_3 uptake with the uptake of sulfuric acid (H_2SO_4) before HNO_3 and HCl can partition

304   into the aqueous aerosol; hence all SO_4^{2-} in the condensed phase will be fully neutralized before any HNO_3, or

305   HCl can partition (Behera et al., 2013). Typical Delhi winter conditions of excess NH_3, high RH, and low T favor

306   gas-to-particle partitioning of NH_3. The principal inorganic chemical reactions that occur in aqueous atmospheric

307 aerosols form pairs of non-volatile NH_4^+ and acid anions (SO_4^{2-}, NO_3^-, and Cl^-) are summarized in reactions R1

308 to R3 (Seinfeld et al., 1998).

309 $$2NH_{3(g)} + H_2SO_{4(g)} \rightleftarrows NH_4^+ + SO_4^{2-} \qquad\qquad\qquad (R1)$$

310 $$NH_{3(g)} + HNO_{3(g)} \rightleftarrows NH_4^+ + NO_3^- \qquad\qquad\qquad (R2)$$

311 $$NH_{3(g)} + HCl_{(g)} \rightleftarrows NH_4^+ + Cl^- \qquad\qquad\qquad (R3)$$

312

313 NH_4^+ and Cl^- (R3), which are favored by low T and high RH, form a reversible equilibrium with NH_3 and HCl

314 (Ianniello et al., 2011; Seinfeld and Pandis, 2016), which was the case during WiFEX. It is likely that high Cl^- in

315 Delhi resulted from gas–to-particle partitioning of HCl into aerosol water in the presence of excess NH_3 (R3),

316 with aqueous phase Cl^- stimulating further water uptake and jointly driving aerosol mass composition and growth

317 through co-condensation (Chen et al., 2022; Gunthe et al., 2021). Hence, to understand the driver of the measured

318 NH_4^+ and the role of aqueous chemistry, we plotted the fraction of the ratio of HCl to Cl^- (HCl/Cl^-) as a function

319 of NH_4^+ concentration and RH in Fig. 4. The decrease in the fraction of HCl/Cl^- is associated with an increase in

320 NH_4^+ concentration at high RH between 70-100 %. The HCl/Cl^- is highly anticorrelated (r = -0.53) with NH_4^+

321 concentration in the presence of high RH (70-100 %), further supporting the view that HCl promotes the increase

322 in the particle fraction of NH_4^+ (49.5 %) with Cl^- (29.7 %) the primary anion.

323 We investigated the directions of local emission sources associated with concentration increases of NH_3,

324 NH_4^+, Cl^- and NH_x through bivariate polar graphs using the OpenAir software (Carslaw and Ropkins, 2012) at the

325 IGIA site. Figure 5 shows the bivariate polar plots of mean NH_3 (Fig. 5a), NH_4^+ (Fig. 5b), Cl^- (Fig. 5c), and total

326 NH_x (Fig. 5d) concentration for the observation period in relation to wind speed and wind direction. The 270-300º

327 sector dominated the wind direction at IGIA (Acharja et al., 2021). Figure 5a shows that the highest NH_3

328 concentration was associated with the winds coming from the east and southeast of the site, where it could have

329 been emitted from dairy farms, including animal houses, yards, and manure storage, as well as by the application

330 to the farmland of urea and other ammoniacal fertilizers, ammoniacal wastes and ruminant urine located at this

331 region (Hindustan Times, 2021; Leytem et al., 2018; Sherlock et al., 1994). Such sources of NH_3 volatilization

332 (Hristov et al., 2011; Laubach et al., 2013) can also explain the higher concentrations of total NH_4^+ (and, by

333 definition NH_x) for air coming from the southeast of the measurement site (Fig. 5b and d). This enhancement in

334 the southeast region is not only affected by emissions but also by meteorology and chemistry. Thus higher NH_3

335 concentration may also be due to the lack of turbulent mixing, which restricts the dilution of plumes from local

336 point sources at lower wind speeds (Ianniello et al., 2010). The bivariate polar plots of NH_4^+ (Fig. 5b) and Cl^-

337 (Fig. 5c) concentration point to the west direction as a principal source for thermodynamic partitioning of NH_3

338 and HCl to the condensed phase to form NH_4^+ and Cl^-. Two industrial sources are located in this direction: the

339 site is impacted by a cluster in northwest Delhi of industrial processes, such as steel pickling industries, and others

340 include metal finishing and electroplating, which are known to be vital HCl emitters (Acharja et al., 2021;

341 Jaiprakash et al., 2017). Near the source, abundant quantities of NH_3 may drive the partitioning of HCl to the

342 condensed phase resulting in high concentrations of NH_4^+ and Cl^- towards the west at lower wind speeds. Thus,

343 high NH_4^+ and Cl^- correspond to the lowest NH_3 concentration region (inverse relation), which can be observed

344 in Fig. 5a, b, and c, highlighting the importance of nearby HCl industrial sources in driving the particle fraction

345 of NH_4^+ and Cl^-.

346 To gain insight into the role of NH_4^+ in the neutralization of anions (SO_4^{2-}, NO_3^- and Cl^-), the aerosol

347 neutralization ratio (ANR) was calculated using the observed data. The ANR is defined as the equivalent ratio of

348 NH_4^+ to the sum of SO_4^{2-}, NO_3^{-} and Cl^- because these species represent the dominant cations and anions in $PM_{2.5}$,

349 respectively. Figure 6 demonstrates, on average, how well the charge balance works between Cl^-, NO_3^- and SO_4^{2-}

350 (in µeq m^{-3}) as the anions and NH_4^+ as the major cation (ANR close to unity), with Cl^- as the most significant

351 anion followed by NO_3^- and SO_4^{2-}. The mean $\pm 1\sigma$ ANR value for $PM_{2.5}$ during the observed period was 0.96 $\pm$

352 0.14. It ranges from a minimum of 0.35 $\pm$ 0.04 to a maximum of 2.31 $\pm$ 0.08. Higher values than unity may indicate

353 the presence of organic acids in the aerosol, which MARGA does not measure (Acharja et al., 2020). Also, high

354 standard error in Fig.6 indicates the possibility of uncertainties associated with the breakthrough of NH_3 spikes on

355 the denuder at high concentration (~ 1 %) (Stieger et al., 2019). However, the good charge balance indicates this

356 wasn't a major issue. There also were certain periods where low concentrations were observed of Cl^- and NO_3^-

357 (03-06 January 2018 and 16-17 January 2018) in Fig. 6. Comparing the model/obs for NH_3, $NH_4^{+,}$ and total NH_x

358 during these periods provides some degree of validation of the model where sulfur chemistry dominates the

359 reaction with NH_3. Figure S4 (in the supplement) shows that model/obs indicates substantial variability which

360 appears to be overestimating NH_3 (model/obs >1) while underestimating total NH_4^+ (model/obs <1) on average

361 in the model.

362 **3.3 Influence of HCl/Cl$^-$ chemistry in WRF-Chem**

363 We further conducted three scenario simulations for the period 7-16 January 2018 (10 days) to explore the

364 potential impacts of the addition of anthropogenic chloride (HCl/Cl$^-$) emissions in the concentrations of NH_3,

365 NH_4^+ and total NH_x. We employ the HCl emissions from trash-burning activities in Delhi, as predicted by Sharma

366 et al. (2019) in our model set-up. We tested the three sensitivity experiments named: No HCl (0 mol km^{-2} h^{-1}),

367 Base Case HCl (3× Sharma et al., 2019; 24.8 mol km^{-2} h^{-1}), and 3×Base HCl (74 mol km^{-2} h^{-1}) scenario, reflecting

368 adjustments which are consistent with the more recent upward adjustments in the amount of waste burned in

369 landfills by Chaudhary et al. (2021) and also to reflect additional industrial HCl sources not accounted for in the

370 inventory. Figure 7 presents the box-whiskers plots for secondary inorganic aerosols and trace gases from the

371 observations (MARGA), and those simulated by the model for the three sensitivity experiments. Daily mean $\pm 1\sigma$

372 values are summarized in Table 2 for three different model scenarios. As can be observed from Fig. 7(a-c),

373 increasing the HCl emissions (Fig. 7g) in the model partitions more NH_3 to the condensed phase due to its high

374 concentrations, reaching maximum mass loadings of NH_4^+ and Cl^- of 70 and 110 µg m^{-3}, respectively, in the

375 3×Base HCl scenario, while increasing the total mean NH_x concentration by 15 µg m^{-3} compared to the No HCl

376 run presumably reflecting the longer residence time of NH_4^+ for near-surface air measurements.

377 The simulated NO_3^- concentration (Fig. 7e) generally exceeds the measurements in all three experiments;

378 since the main neutralizing species for NO_3^- is NH_4^+, it is controlled via the equilibrium between NO_3^-, HNO_3, and

379 NH_3, but also the competition with HCl for free NH_3. Simulated HNO_3 is significantly underestimated (by ~3 µg

380 m^{-3}) (Fig. 7h) by the model compared to the observations. As a consequence, the model suggests that NO_3^-

381 formation from gaseous NH_3 and HNO_3 cannot occur. The gas fraction of observed HNO_3 will be determined by

382 aerosol pH and liquid water content based on NH_3 and NO_3^- availability (Nenes et al., 2020). The over-prediction

383 of NH_3 concentration in the model compared with the observations generates more NO_3^- (and simultaneously

384 reduces HNO_3), with the total fraction of $HNO_3 + NO_3^-$ (THNO$_3$) concentration in the model also exceeding the

385   observed THNO$_3$, which is more strongly affected by reducing the NH$_3$ emissions in the model (Fig. S5 in the

386   Supplement). On average, THNO$_3$ reduced by only 0.38 µg m^{-3} in 3×Base HCl compared to the No HCl run. But

387   reducing NH$_3$ emissions by a factor of 3 (-3×NH$_3$_EMI) in the 3×Base HCl scenario reduced mean THNO$_3$ by a

388   further 4.71 µg m^{-3}. The extent of partitioning and accumulation of NH$_4$NO$_3$ depends on T, aerosol water, pH, as

389   well as NH$_3$ availability (Nenes et al., 2020). Our model simulations find that the presence of HCl/Cl$^-$ does not

390   significantly alter THNO$_3$ but that the excess NH$_3$ with missing chloride chemistry is a major contributor and will

391   lead to mismatches in the model between measured simulated gas and particulate matter concentrations.

392   The simulated SO$_4^{2-}$ concentration (Fig. 7f) was underestimated (by ∼ 7.5 µg m^{-3}), while gas-phase SO$_2$

393   Fig. 7i) was found to be overestimated by about 16 µg m^{-3} in all three experiments compared with the observations.

394   This may be caused by the fact that the drivers for typical sulfate production via OH or aqueous H$_2$O$_2$ oxidation

395   pathway are likely to be wrong in the model. The missing chemistry may underly this mismatch and requires

396   further sensitivity studies considering different SO$_2$ oxidation pathways. This requires further study, such as

397   scenario evaluation of altered SO$_2$ emissions in the model, to examine the main pathway(s) for SO$_2$ to SO$_4^{2-}$

398   conversion. Measurements of OH and other radicals in Delhi are currently lacking, making it difficult to constrain

399   the associated chemical schemes. To investigate the further impact of 3×Base HCl in the model, uptake of gaseous

400   NH$_3$ to form NH$_4^+$ and Cl$^-$ was analyzed via a strong correlation coefficient values of r = 0.84 for NH$_4^+$/NH$_x$ with

401   Cl$^-$ concentration, indicating a fraction of gas-to-particle conversion in the model correlates well with the Cl$^-$

402   concentration and was reasonably well simulated in the 3×Base HCl run.

403   **3.4 Comparison of the temporal variation in NH$_3$, NH$_4^+$, and NH$_x$ using WRF-Chem (HCl/Cl$^-$) and**
404   **MARGA**

405   **3.4.1 Diurnal variation**

406   Here, diurnal variations of monitored aerosol compounds and gases were analysed to investigate the gas-to-

407   particle conversion of NH$_3$ in the model. We analyzed the simulation results of the 3×Base HCl run. The diurnal

408   variations for NH$_3$ and NH$_4^+$ are controlled mainly by thermodynamic gas-to-particle partitioning, boundary layer

409   mixing, emission and deposition processes, along with vertical and horizontal advection (Meng et al., 2018).

410   Figure 8 (top) presents the diurnal variations of NH$_3$ and NH$_4^+$ (in µg m^{-3}) along with particulate NH$_4^+$, Cl$^-$, NO$_3^-$

411   , SO$_4^2$, SO$_2$, HCl, and HNO$_3$ concentrations (in µeq m^{-3}) measured (Fig. 8a (top)) and modeled (Fig. 8b (top))

412   along with its meteorological parameters such as T and RH (Fig. 8 (bottom)). We adopted diurnal variation in

413   emissions from Jena et al. (2021) based on boundary layer mixing. It can be seen in Fig. 8a (top and bottom) that

414   a much bigger peak in NH$_3$ concentration is observed in the daytime than the modeled (despite turbulence

415   differences), indeed suggesting a much stronger NH$_3$ in the middle of the day (11:00-01:00 h). As evaporation

416   proceeds mainly in the morning (08:00-12:00) getting warmer, the peak is near midday (11:00-13:00 h), rather

417   than in the afternoon (13:00-14:00 h) when warmest, similar to what was also observed in Sutton et al. (1998).

418   Indeed, the decreasing NH$_4^+$ and Cl$^-$ during the late morning (10:00 h) corresponds to the increasing NH$_3$ peak,

419   which reflects the fact that warming promotes the shift of aerosols to the gas phase. Ammonium decreases more

420   than NH$_3$ during the day, as this also evaporates to form NH$_3$. Similarly, Cl$^-$ evaporates during the day since the

421   HCl concentration increases. However, it can be seen that NO$_3^-$ and SO$_4^{2-}$ are slightly changed diurnally, inferring

422   longer range transport perhaps, whereas HCl and Cl$^-$ are from more local sources. The diurnal variability in gases

423   and aerosols in 3×Base HCl simulations in Fig. 8b (top) is primarily controlled by the planetary boundary layer

424   mixing, meteorology/dispersion, environment (T and RH in Fig. 8b (bottom)), and transport. So presumably,

425   maximum NH_3 at 08:00 h is due to limited turbulence/boundary layer, with dilution by mixing after 08:00 h.

426   However, the model is able to represent well the diurnal variation of NH_4^+ and Cl^- both in terms of amount and

427   pattern, which was not the case in the No HCl run where NH_4^+ was observed to be flat in Section 1. During the

428   hours of 09:00 and 11:00 h, when measured NH_3 rises, the model predicts a large decrease in NH_3, while during

429   19:00-23:00 h, when measured NH_3 decreases, the model predicts a large increase. Furthermore, the modeled HCl

430   and HNO_3 are very low compared to the measurements, whereas SO_2 concentration matches well with the

431   observations. It can be seen that NO_3^- and SO_4^{2-} are flat in the model. This highlights the need to develop accurate

432   diurnal variability in NH_3 emissions over this region.

433   Figure 9 presents the differences in diurnal variation of mean NH_3 (Fig. 9a), NH_4^+ (Fig. 9b), and total

434   NH_x (Fig. 9c) concentration for the three sensitivity experiments. While the simulated NH_3 concentrations

435   decrease in the 3×Base HCl compared to the No HCl and Base Case HCl run (Table 2), none of the model

436   experiments capture the diurnal cycle of NH_3. Higher levels of observed NH_3 during daytime and modeled NH_3

437   during night-time highlight the need to improve diurnal variability in NH_3 emissions over this region based on the

438   nature and strength of the actual sources. Between the No HCl and the 3xBase HCl run, the NMB for NH_3 reduced

439   from 1.38 to 1.13, and NMB for NH_4^+ systematically improved from -0.61 to -0.03. In contrast, NMB for total

440   NH_x increased from 0.12 to 0.39. Table 3 summarizes the statistical indicators for the three sensitivity

441   experiments. An increase in HCl emissions in the 3×Base HCl leads to a higher mass concentration of NH_4^+ and

442   Cl^-, which also increases total mean NH_x concentration by 22.4 µg m^{-3}, presumably reflecting the longer

443   atmospheric lifetime of NH_4^+ compared with NH_3. We find consistent high bias in all the simulations for NH_3,

444   which is highest during the early morning and at night-time. In order to better understand the relationship between

445   NH_3, NH_4^+ and NH_x concentrations in the diurnal profile of model, one sensitivity study is conducted in the best

446   case HCl experiment to simulate the response of NH_x concentrations by changing NH_3 emissions. In these

447   simulations, only NH_3 emissions were reduced further by a factor of 3 (-3×NH$_3$_EMI) in the 3×Base HCl

448   experiment, while all other processes and chemical schemes were unchanged. Figure S6 in the Supplement shows

449   the diel profile of model/obs ratio for NH_3 (Fig. S6a), NH_4^+ (Fig. S6b), and total NH_x (Fig. S6c) concentration

450   simulated with the 3×Base HCl and -3×NH$_3$_EMI scenario. Reducing NH_3 emissions in the model (-3×NH$_3$_EMI)

451   significantly improves model-measurement agreement for NH_3 (mean model/obs = 1.9), NH_4^+ (mean model/obs

452   = 0.9), and total NH_x concentration (mean model/obs = 1.2) compared to the 3×Base HCl run, further suggesting

453   that the longer lifetime of NH_4^+ may be the controlling driver for the total NH_x concentration in the model.

454   **3.4.2 Variation of daily means**

455   Figure S7 in the Supplement illustrates a time-series graph that compares daily mean NH_3 (Fig. S7a), NH_4^+ (Fig.

456   S7b), and total NH_x concentrations (Fig. S7c) for the three sensitivity experiments, and Table 2 shows the mean

457   ± 1σ of these variables. The results show that compared to the No HCl run, NH_3 mean concentrations decreased

458   by 2 µg m^{-3} in the Base Case HCl and decreased by a further 3.2 µg m^{-3} in the 3×Base HCl run. On the contrary,

459   NH_4^+ mean concentration increases in the Base Case HCl by 7.5 µg m^{-3} and further increases by 13.1 µg m^{-3}

460   (3×Base HCl). This decrease in NH_3 is associated with the enhanced gas-to-particle conversion of NH_3 to NH_4^+.

461   Associated with these changes, total mean NH_x also increased by 5.5 and 9.8 µg m^{-3} in the Base Case HCl and

462   3×Base HCl, respectively, compared to the No HCl. This is likely due to associated increases in the atmospheric

463   lifetime of NH_x with respect to deposition as the partitioning shifted from the faster depositing gas phase to the
464   aerosol phase. The lifetime of NH_3 is very short, a few hours, while that of NH_4^+ is 1 to 15 days (Aneja et al.,
465   1998; Nair and Yu, 2020; Pawar et al., 2021; Wang et al., 2020a).

466   To understand further the overestimation of total NH_x in the daily mean variation by the model, we
467   compared 3×Base HCl and -3×NH_3_EMI sensitivity experiment. Figure 10 shows the ratio of model/obs for NH_3
468   (Fig. 10a), NH_4^+ (Fig. 10b) and total NH_x (Fig. 10c) concentration. It can be seen that the model-measurement
469   agreement improves significantly (model/obs closer to 1) after reducing NH_3 emissions for all three metrics. -
470   3×NH_3_EMI would reduce the mean NH_3, NH_4^+, and total NH_x concentration by ∼8.1 µg m^{-3}, 3.2 µg m^{-3}, and
471   11.3 µg m^{-3}, respectively, compared to the 3×Base HCl run. Even though reducing NH_3 emissions, it is still
472   sufficient to react rapidly with the varying HCl in the sensitivity experiments contributing to an increase in NH_4^+.
473   As can be seen in Fig. 10b, initially, NH_4^+ is somewhat lower, but it increases later and matches the 3×Base HCl
474   run. This suggests that NH_4^+ formation in the model is more sensitive to changes in HCl than changes in NH_3
475   emission, while total NH_x agrees well by reducing the NH_3 emissions. In general, CTMs have higher NH_3
476   concentration than observations, further supporting models having too much NH_3. A few factors might contribute
477   to the model discrepancies for NH_3: there are uncertainties in the emission inventory of the bottom-up approach
478   of NH_3, and the model does not currently include the bidirectional exchange of NH_3 with surfaces, such as dew
479   and fog water. Also, model does not have accurate industrial sources of HCl emission. Diurnal emission profiles
480   are uncertainty for both NH_3 and HCl. Furthermore, gas-to-particle partitioning associated with SO_2 oxidation
481   pathways in the model is not correct at present.

482   **4. Conclusions**

483   In this study, we have evaluated for the first time in South Asia the performance of a chemical transport model
484   (WRF-Chem) in modeling NH_3, NH_4^+, and total NH_x, by comparing against the WiFEX measurements
485   (MARGA). In daily means, we find NH_3 is significantly overestimated by the model, NH_4^+ was underestimated
486   while simulated total NH_x agreed well with the measurement, indicating incorrect gas-to-particle partitioning
487   along with missing chemical process may impact this mismatch in the model. The ability of the model to
488   accurately describe the gas-to-particle partitioning of the MARGA was evaluated by the fraction of total NH_x (=
489    $NH_3 + NH_4^+$) in the particulate phase (NH_4^+/NH_x). A strong relation of MARGA NH_4^+/NH_x was observed with
490   dominant anion (Cl$^-$) (r = 0.79), whereas the standard model showed a strong correlation between NH_4^+/NH_x with
491   dominant anion (SO_4^{2-}) (r = 0.77), pointing to the missing chloride (HCl/Cl$^-$) chemistry in the model.

492   We incorporated HCl/Cl$^-$ emissions in the model and conducted three sensitivity experiments of varying
493   HCl emissions, named as No HCl (0 mol km^{-2} h^{-1}), Base Case HCl (3× Sharma et al., 2019; 24.8 mol km^{-2} h^{-1})
494   and 3×Base HCl (74 mol km^{-2} h^{-1}) run. The revised model shows that by adding HCl emissions more NH_x was
495   partitioned to the condensed phase improving agreement with the observations. 3×Base HCl was able to represent
496   well the diurnal variation of NH_4^+ and Cl$^-$ both in terms of amount and pattern with improved NMB for NH_3.
497   Additional sensitivities tests in changing NH_3 emissions (reduction by a factor of 3) in the 3×Base HCl also
498   improved NH_3, NH_4^+, and NH_x concentrations. We find excess NH_3 along with longer lifetime of NH_4^+ may act
499   as a controlling driver for NH_x overestimation in the model. These results highlight the need to include correct
500   industrial sources of HCl emissions along with appropriate emissions of NH_3 to reduce biases in NH_x. Developing
501   the appropriate NH_3 emissions using country-specific emission inventories, which are currently under

development as part of the Global Challenges Research Fund (GCRF), South Asian Nitrogen Hub (SANH). Also, there is potential to develop top-down constraints on NH_3 emissions by taking inference from the satellite, model, and ground-based observations. Challenges remain in simulating NH_3 as a contributor to particulate matter due to temporal factors in ammonia peaks including the role of fog and dew where more work is needed. This work also suggests model improvements to SO_2 oxidation pathways could improve NH_x partitioning.

Data availability

The $0.1^\circ \times 0.1^\circ$ emission grid maps can be downloaded from the EDGAR website on https://edgar.jrc.ec.europa.eu/htap_v2/index.php?SECURE=_123 per year per sector. Gridded emissions in t y^{-1} on a $0.1^\circ \times 0.1^\circ$ for HCl emissions can be downloaded from Mendeley data: http://dx.doi.org/10.17632/546t9249bv.1. The model data is available at Aditya, Indian Institute of Tropical Meteorology (IITM) super-computer and can be provided upon request to the corresponding author. The observational and meteorological data of WiFEX are available by contacting the corresponding author.

Author contributions

SDG designed the research; PVP performed the WRF-Chem model simulations and led the analysis; PA and RK contributed to data collection and its quality control and assurance; GG, RK, and PG helped with the model set up; PVP and SDG wrote the paper with contributions from all co-authors.

Competing interests

The authors declare that they have no conflict of interest.

Acknowledgments

We thank the Director, IITM, for his continuous support and encouragement. IITM is funded by the Ministry of Earth Sciences (MoES), Government of India. We wish to thank the MoES for supporting the WiFEX campaign. The lead author's fellowship was supported by the National Supercomputing Mission (NSM) program grant at C-DAC, and Ph.D. fees are covered by the Natural Environment Research Council (NERC) of UK Research and Innovation (UKRI)-Global Challenges Research Fund (GCRF), South Asian Nitrogen Hub (SANH), and we are grateful to the Executive Director and the Director-General of C-DAC and the SANH Director and Chair of the Executive Board. We acknowledge the availability of CPCB-NO_x, NO_2, and O_3 data from the CPCB web portal (https://app.cpcbccr.com/ccr, last access: 1 December 2021). We wish to acknowledge the National Center for Atmospheric Research is sponsored by the National Science Foundation.

5. References

Acharja, P., Ali, K., Trivedi, D. K., Safai, P. D., Ghude, S., Prabhakaran, T. and Rajeevan, M.: Characterization

of atmospheric trace gases and water soluble inorganic chemical ions of PM1 and PM2.5 at Indira Gandhi International Airport, New Delhi during 2017–18 winter, Sci. Total Environ., 729, 138800, doi:10.1016/j.scitotenv.2020.138800, 2020.

Acharja, P., Ali, K., Ghude, S. D., Sinha, V., Sinha, B., Kulkarni, R., Gultepe, I. and Nair, M.: Chemosphere Enhanced secondary aerosol formation driven by excess ammonia during fog episodes, Chemosphere, 289(November 2021), 133155, doi:10.1016/j.chemosphere.2021.133155, 2021.

Ali, K., Acharja, P., Trivedi, D. K., Kulkarni, R., Pithani, P., Safai, P. D., Chate, D. M., Ghude, S., Jenamani, R. K. and Rajeevan, M.: Characterization and source identification of PM 2.5 and its chemical and carbonaceous constituents during Winter Fog Experiment 2015–16 at Indira Gandhi International Airport, Delhi, Sci. Total Environ., 662, 687–696, doi:10.1016/j.scitotenv.2019.01.285, 2019.

Aneja, V. P., Murray, G. C. and Southerland, J.: Atmospheric nitrogen compounds: Emissions, transport, transformation, deposition, and assessment, EM Air Waste Manag. Assoc. Mag. Environ. Manag., 22–25, 1998.

Behera, S. N., Sharma, M., Aneja, V. P. and Balasubramanian, R.: Ammonia in the atmosphere: a review on emission sources, atmospheric chemistry and deposition on terrestrial bodies, Environ. Sci. Pollut. Res., 20(11), 8092–8131, doi:10.1007/s11356-013-2051-9, 2013.

Bucaram, C. J. and Bowman, F. M.: Wrf-chem modeling of summertime air pollution in the northern great plains: Chemistry and aerosol mechanism intercomparison, Atmosphere (Basel)., 12(9), doi:10.3390/atmos12091121, 2021.

Carslaw, D. C. and Ropkins, K.: Openair - An r package for air quality data analysis, Environ. Model. Softw., 27–28(July 2019), 52–61, doi:10.1016/j.envsoft.2011.09.008, 2012.

Chaudhary, P., Garg, S., George, T., Shabin, M., Saha, S., Subodh, S. and Sinha, B.: Underreporting and open burning – the two largest challenges for sustainable waste management in India, Resour. Conserv. Recycl., 175, 105865, doi:https://doi.org/10.1016/j.resconrec.2021.105865, 2021.

Chen, Y., Wang, Y., Nenes, A., Wild, O., Song, S., Hu, D., Liu, D., He, J., Hildebrandt Ruiz, L., Apte, J. S., Gunthe, S. S. and Liu, P.: Ammonium Chloride Associated Aerosol Liquid Water Enhances Haze in Delhi, India, Environ. Sci. Technol., 56(11), 7163–7173, doi:10.1021/acs.est.2c00650, 2022.

Clarisse, L., Clerbaux, C., Dentener, F., Hurtmans, D. and Coheur, P. F.: Global ammonia distribution derived from infrared satellite observations, Nat. Geosci., 2(7), 479–483, doi:10.1038/ngeo551, 2009.

Clarisse, L., Shephard, M. W., Dentener, F., Hurtmans, D., Cady-Pereira, K., Karagulian, F., Van Damme, M., Clerbaux, C. and Coheur, P. F.: Satellite monitoring of ammonia: A case study of the San Joaquin Valley, J. Geophys. Res. Atmos., 115(13), 1–15, doi:10.1029/2009JD013291, 2010.

CPCB: Annual Report 2014-15., 2014.

CPCB: Annual Report Annual Report., 2020.

Van Damme, M., Clarisse, L., Whitburn, S., Hadji-Lazaro, J., Hurtmans, D., Clerbaux, C. and Coheur, P. F.: Industrial and agricultural ammonia point sources exposed, Nature, 564(7734), 99–103, doi:10.1038/s41586-018-0747-1, 2018.

Datta, A., Sharma, S. K., Harit, R. C., Kumar, V., Mandal, T. K. and Pathak, H.: Ammonia emission from subtropical crop land area in india, Asia-Pacific J. Atmos. Sci., 48(3), 275–281, doi:10.1007/s13143-012-0027-1, 2012.

Duan, X., Yan, Y., Peng, L., Xie, K., Hu, D., Li, R. and Wang, C.: Role of ammonia in secondary inorganic

572 aerosols formation at an ammonia-rich city in winter in north China: A comparative study among industry, urban,

573 and rural sites, Environ. Pollut., 291(May), 118151, doi:10.1016/j.envpol.2021.118151, 2021.

574 Ellis, R. A., Murphy, J. G., Markovic, M. Z., Vandenboer, T. C., Makar, P. A., Brook, J. and Mihele, C.: The

575 influence of gas-particle partitioning and surface-atmosphere exchange on ammonia during BAQS-Met, Atmos.

576 Chem. Phys., 11(1), 133–145, doi:10.5194/acp-11-133-2011, 2011.

577 FINNv1.5: FINN Data, [online] Available from: http://bai.acom.ucar.edu/Data/fire/ (Accessed 15 April 2019),

578 n.d.

579 Freitas, S. R., Longo, K. M., Chatfield, R., Latham, D., Silva Dias, M. A. F., Andreae, M. O., Prins, E., Santos, J.

580 C., Gielow, R. and Carvalho Jr., J. A.: Including the sub-grid scale plume rise of vegetation fires in low resolution

581 atmospheric transport models, Atmos. Chem. Phys., 7(13), 3385–3398, doi:10.5194/acp-7-3385-2007, 2007.

582 Georgiou, G. K., Christoudias, T., Proestos, Y., Kushta, J., Hadjinicolaou, P. and Lelieveld, J.: Air quality

583 modelling in the summer over the eastern Mediterranean using WRF-Chem: chemistry and aerosol mechanism

584 intercomparison, Atmos. Chem. Phys., 18(3), 1555–1571, doi:10.5194/acp-18-1555-2018, 2018.

585 Ghude, S., Kumar, R., Jena, C., Debnath, S., Kulkarni, R., Alessandrini, S., Biswas, M., Kulkrani, S., Pithani, P.,

586 Kelkar, S., Sajjan, V., Chate, D., Soni, V., Singh, S., Nanjundiah, R. and Rajeevan, M.: Evaluation of PM2.5

587 Forecast using Chemical Data Assimilation in the WRF-Chem Model: A Novel Initiative Under the Ministry of

588 Earth   Sciences   Air   Quality   Early   Warning   System   for   Delhi,   India,   Curr.   Sci.,   118,

589 doi:10.18520/cs/v118/i11/1803-1815, 2020.

590 Ghude, S. D.: Premature mortality in India due to PM2.5 and ozone exposure, Geophys. Res. Lett., 1–8,

591 doi:10.1002/2013GL058740.Received, 2016.

592 Ghude, S. D., Fadnavis, S., Beig, G., Polade, S. D. and van der A, R. J.: Detection of surface emission hot spots,

593 trends, and seasonal cycle from satellite-retrieved NO $_2$ over India, J. Geophys. Res., 113(D20), D20305,

594 doi:10.1029/2007JD009615, 2008a.

595 Ghude, S. D., Jain, S. L., Arya, B. C., Beig, G., Ahammed, Y. N., Kumar, A. and Tyagi, B.: Ozone in ambient air

596 at a tropical megacity, Delhi: Characteristics, trends and cumulative ozone exposure indices, J. Atmos. Chem.,

597 60(3), 237–252, doi:10.1007/s10874-009-9119-4, 2008b.

598 Ghude, S. D., Van der A, R. J., Beig, G., Fadnavis, S. and Polade, S. D.: Satellite derived trends in NO2 over the

599 major global hotspot regions during the past decade and their inter-comparison, Environ. Pollut., 157(6), 1873–

600 1878, doi:10.1016/j.envpol.2009.01.013, 2009.

601 Ghude, S. D., Lal, D. M., Beig, G., van der A, R. and Sable, D.: Rain-Induced Soil NO $_x$ Emission From India

602 During the Onset of the Summer Monsoon: A Satellite Perspective, J. Geophys. Res., 115(D16), D16304,

603 doi:10.1029/2009JD013367, 2010.

604 Ghude, S. D., Pfister, G. G., Jena, C. K., Emmons, L. K., Kumar, R. and van der A, R. J.: Satellite constraints of

605 Nitrogen Oxide (NOX) emissions from India based on OMI observations and WRF-Chem simulations, Geophys.

606 Res. Lett., 40(x), 423–428, doi:10.1029/2012gl053926, 2012.

607 Ghude, S. D., Kulkarni, S. H., Jena, C., Pfister, G. G., Beig, G., Fadnavis, S. and Van Der, R. J.: Application of

608 satellite observations for identifying regions of dominant sources of nitrogen oxides over the indian subcontinent,

609 J. Geophys. Res. Atmos., 118(2), 1075–1089, doi:10.1029/2012JD017811, 2013.

610 Ghude, S. D., Bhat, G. S., Prabhakaran, T., Jenamani, R. K., Chate, D. M., Safai, P. D., Karipot, A. K., Konwar,

611 M., Pithani, P., Sinha, V., Rao, P. S. P., Dixit, S. A., Tiwari, S., Todekar, K., Varpe, S., Srivastava, A. K., Bisht,

D. S., Murugavel, P., Ali, K., Mina, U., Dharua, M., Rao, Y. J., Padmakumari, B., Hazra, A., Nigam, N., Shende, U., Lal, D. M., Chandra, B. P., Mishra, A. K., Kumar, A., Hakkim, H., Pawar, H., Acharja, P., Kulkarni, R., Subharthi, C., Balaji, B., Varghese, M., Bera, S. and Rajeevan, M.: Winter fog experiment over the Indo-Gangetic plains of India, Curr. Sci., 112(4), doi:10.18520/cs/v112/i04/767-784, 2017.

Ghude, S. D., Kumar, R., Govardhan, G., Jena, C., Nanjundiah, R. S. and Rajeevan, M.: New Delhi: air-quality warning system cuts peak pollution, Nature, 602(7896), 211, doi:10.1038/D41586-022-00332-Y, 2022.

Ginoux, P., Chin, M., Tegen, I., Goddard, T. and In-, G.: Sources and distribution of dust aerosols simulated with the GOCART model, J. Geophys. Res., 106, 20255–20273, doi:https://doi.org/10.1029/2000JD000053, 2001.

Gu, B., Zhang, L., Dingenen, R. Van, Vieno, M., Grinsven, H. J. Van, Zhang, X., Zhang, S., Chen, Y., Wang, S., Ren, C., Rao, S., Holland, M., Winiwarter, W., Chen, D., Xu, J. and Sutton, M. A.: Abating ammonia is more cost-effective than nitrogen oxides for mitigating PM2.5 air pollution, Science (80-.)., 374(6568), 758–762, doi:10.1126/science.abf8623, 2021.

Guenther, A., Karl, T., Harley, P., Wiedinmyer, C., Palmer, P. I. and Geron, C.: Estimates of global terrestrial isoprene emissions using MEGAN (Model of Emissions of Gases and Aerosols from Nature), Atmos. Chem. Phys., 6(11), 3181–3210, doi:10.5194/acp-6-3181-2006, 2006.

Gunthe, S. S., Liu, P., Panda, U., Raj, S. S., Sharma, A., Darbyshire, E., Reyes-Villegas, E., Allan, J., Chen, Y., Wang, X., Song, S., Pöhlker, M. L., Shi, L., Wang, Y., Kommula, S. M., Liu, T., Ravikrishna, R., McFiggans, G., Mickley, L. J., Martin, S. T., Pöschl, U., Andreae, M. O. and Coe, H.: Enhanced aerosol particle growth sustained by high continental chlorine emission in India, Nat. Geosci., 14(2), 77–84, doi:10.1038/s41561-020-00677-x, 2021.

Gupta, M. and Mohan, M.: Validation of WRF/Chem model and sensitivity of chemical mechanisms to ozone simulation over megacity Delhi, Atmos. Environ., 122, 220–229, doi:10.1016/j.atmosenv.2015.09.039, 2015.

Hindustan Times: 66 dairies, six dyeing units shut down in east Delhi, Hindustan Times, 6th July, 2021.

Hristov, A. N., Hanigan, M., Cole, A., Todd, R., McAllister, T. A., Ndegwa, P. M. and Rotz, A.: Review: Ammonia emissions from dairy farms and beef feedlots, Can. J. Anim. Sci., 91(1), 1–35, doi:10.4141/CJAS10034, 2011.

Huang, X., Song, Y., Li, M., Li, J., Huo, Q., Cai, X., Zhu, T., Hu, M. and Zhang, H.: A high-resolution ammonia emission inventory in China, Global Biogeochem. Cycles, 26(1), 1–14, doi:10.1029/2011GB004161, 2012.

Ianniello, A., Spataro, F., Esposito, G., Allegrini, I., Rantica, E., Ancora, M. P., Hu, M. and Zhu, T.: Occurrence of gas phase ammonia in the area of Beijing (China), Atmos. Chem. Phys., 10(19), 9487–9503, doi:10.5194/acp-10-9487-2010, 2010.

Ianniello, A., Spataro, F., Esposito, G., Allegrini, I., Hu, M. and Zhu, T.: Chemical characteristics of inorganic ammonium salts in PM2.5 in the atmosphere of Beijing (China), Atmos. Chem. Phys., 11(21), 10803–10822, doi:10.5194/acp-11-10803-2011, 2011.

Jaiprakash, Singhai, A., Habib, G., Raman, R. S. and Gupta, T.: Chemical characterization of PM1.0 aerosol in Delhi and source apportionment using positive matrix factorization, Environ. Sci. Pollut. Res., 24(1), 445–462, doi:10.1007/s11356-016-7708-8, 2017.

Jena, C., Ghude, S., Kulkarni, R., Debnath, S., Kumar, R., Soni, V. K., Acharja, P., Kulkarni, S., Khare, M., Kaginalkar, A., Chate, D., Ali, K., Nanjundiah, R. and Rajeevan, M.: Evaluating the sensitivity of fine particulate matter (PM_{2.5}) simulations to chemical mechanism in Delhi, Atmos. Chem. Phys.

Discuss., (3), 1–28, doi:10.5194/acp-2020-673, 2020.

Jena, C., Ghude, S. D., Kumar, R., Debnath, S., Govardhan, G., Soni, V. K., Kulkarni, S. H., Beig, G., Nanjundiah, R. S. and Rajeevan, M.: Performance of high resolution (400 m) PM2.5 forecast over Delhi, Sci. Rep., 11(1), 1–9, doi:10.1038/s41598-021-83467-8, 2021.

Knote, C., Hodzic, A. and Jimenez, J. L.: The effect of dry and wet deposition of condensable vapors on secondary organic aerosols concentrations over the continental US, Atmos. Chem. Phys., 15(1), 1–18, doi:10.5194/acp-15-1-2015, 2015.

Kulkarni, S. H., Ghude, S. D., Jena, C., Karumuri, R. K., Sinha, B., Sinha, V., Kumar, R., Soni, V. K. and Khare, M.: How Much Does Large-Scale Crop Residue Burning Affect the Air Quality in Delhi?, Environ. Sci. Technol., 54(8), 4790–4799, doi:10.1021/acs.est.0c00329, 2020.

Kumar, A., Hakkim, H., Ghude, S. D. and Sinha, V.: Probing wintertime air pollution sources in the Indo-Gangetic Plain through 52 hydrocarbons measured rarely at Delhi & Mohali, Sci. Total Environ., 801, 149711, doi:https://doi.org/10.1016/j.scitotenv.2021.149711, 2021.

Kumar, R., Barth, M. C., Pfister, G. G., Delle Monache, L., Lamarque, J. F., Archer-Nicholls, S., Tilmes, S., Ghude, S. D., Wiedinmyer, C., Naja, M. and Walters, S.: How Will Air Quality Change in South Asia by 2050?, J. Geophys. Res. Atmos., 123(3), 1840–1864, doi:10.1002/2017JD027357, 2018.

Kumar, R., Ghude, S. D., Biswas, M., Jena, C., Alessandrini, S., Debnath, S., Kulkarni, S., Sperati, S., Soni, V. K., Nanjundiah, R. S. and Rajeevan, M.: Enhancing Accuracy of Air Quality and Temperature Forecasts During Paddy Crop Residue Burning Season in Delhi Via Chemical Data Assimilation, J. Geophys. Res. Atmos., 125(17), 1–16, doi:10.1029/2020JD033019, 2020.

Kuttippurath, J., Singh, A., Dash, S. P., Mallick, N., Clerbaux, C., Van Damme, M., Clarisse, L., Coheur, P. F., Raj, S., Abbhishek, K. and Varikoden, H.: Record high levels of atmospheric ammonia over India: Spatial and temporal analyses, Sci. Total Environ., 740, 139986, doi:10.1016/j.scitotenv.2020.139986, 2020.

Lan, Z., Lin, W., Pu, W. and Ma, Z.: Measurement report: Exploring NH3behavior in urban and suburban Beijing: Comparison and implications, Atmos. Chem. Phys., 21(6), 4561–4573, doi:10.5194/acp-21-4561-2021, 2021.

Laubach, J., Taghizadeh-Toosi, A., Gibbs, S. J., Sherlock, R. R., Kelliher, F. M. and Grover, S. P. P.: Ammonia emissions from cattle urine and dung excreted on pasture, Biogeosciences, 10(1), 327–338, doi:10.5194/bg-10-327-2013, 2013.

Leytem, A. B., Bjorneberg, D. L., Rotz, C. A., Moraes, L. E., Kebreab, E. and Dungan, R. S.: Ammonia emissions from dairy lagoons in the western U.S., Trans. ASABE, 61(3), 1001–1015, doi:10.13031/trans.12646, 2018.

Li, L., Chen, Z. M., Zhang, Y. H., Zhu, T., Li, S., Li, H. J., Zhu, L. H. and Xu, B. Y.: Heterogeneous oxidation of sulfur dioxide by ozone on the surface of sodium chloride and its mixtures with other components, J. Geophys. Res. Atmos., 112(18), 1–13, doi:10.1029/2006JD008207, 2007.

Makkonen, U., Virkkula, A., Mäntykenttä, J., Hakola, H., Keronen, P., Vakkari, V. and Aalto, P. P.: Semi-continuous gas and inorganic aerosol measurements at a Finnish urban site: comparisons with filters, nitrogen in aerosol and gas phases, and aerosol acidity, Atmos. Chem. Phys., 12(12), 5617–5631, doi:10.5194/acp-12-5617-2012, 2012.

Mandal, T. K., Saxena, M., Rohtash, Sharma, S. K., Gupta, N. C., Kumar, M. and Saraswati: Characteristics of ambient ammonia over Delhi, India, Meteorol. Atmos. Phys., 124(1–2), 67–82, doi:10.1007/s00703-013-0299-8, 2013.

692 Meng, Z., Xu, X., Lin, W., Ge, B., Xie, Y., Song, B., Jia, S., Zhang, R., Peng, W., Wang, Y., Cheng, H., Yang,
693 W. and Zhao, H.: Role of ambient ammonia in particulate ammonium formation at a rural site in the North China
694 Plain, Atmos. Chem. Phys., 18(1), 167–184, doi:10.5194/acp-18-167-2018, 2018.

695 Metzger, S., Mihalopoulos, N. and Lelieveld, J.: Importance of mineral cations and organics in gas-aerosol
696 partitioning of reactive nitrogen compounds: Case study based on MINOS results, Atmos. Chem. Phys., 6(9),
697 2549–2567, doi:10.5194/acp-6-2549-2006, 2006.

698 Móring, A., Hooda, S., Raghuram, N., Adhya, T. K., Ahmad, A., Bandyopadhyay, S. K., Barsby, T., Beig, G.,
699 Bentley, A. R., Bhatia, A., Dragosits, U., Drewer, J., Foulkes, J., Ghude, S. D., Gupta, R., Jain, N., Kumar, D.,
700 Kumar, R. M., Ladha, J. K., Mandal, P. K., Neeraja, C. N., Pandey, R., Pathak, H., Pawar, P., Pellny, T. K., Poole,
701 P., Price, A., Rao, D. L. N., Reay, D. S., Singh, N. K., Sinha, S. K., Srivastava, R. K., Shewry, P., Smith, J.,
702 Steadman, C. E., Subrahmanyam, D., Surekha, K., Venkatesh, K., Varinderpal-Singh, Uwizeye, A., Vieno, M.
703 and Sutton, M. A.: Nitrogen Challenges and Opportunities for Agricultural and Environmental Science in India,
704 Front. Sustain. Food Syst., 5, 13, doi:10.3389/fsufs.2021.505347, 2021.

705 Nair, A. A. and Yu, F.: Quantification of atmospheric ammonia concentrations: A review of its measurement and
706 modeling, Atmosphere (Basel)., 11(10), doi:10.3390/atmos11101092, 2020.

707 Nenes, A., Pandis, S. N., Weber, R. J. and Russell, A.: Aerosol pH and liquid water content determine when
708 particulate matter is sensitive to ammonia and nitrate availability, Atmos. Chem. Phys., 20(5), 3249–3258,
709 doi:10.5194/acp-20-3249-2020, 2020.

710 NIVDANGE, S., Jena, C. and Pawar, P.: Nationwide CoViD-19 lockdown impact on air quality in India,
711 MAUSAM, 73(1), 115–128, doi:10.54302/mausam.v73i1.1475, 2022.

712 Pawar, P. V., Ghude, S. D., Jena, C., Móring, A., Sutton, M. A., Kulkarni, S., Lal, D. M., Surendran, D., Van
713 Damme, M., Clarisse, L., Coheur, P.-F., Liu, X., Govardhan, G., Xu, W., Jiang, J. and Adhya, T. K.: Analysis of
714 atmospheric ammonia over South and East Asia based on the MOZART-4 model and its comparison with satellite
715 and surface observations, Atmos. Chem. Phys., 21(8), 6389–6409, doi:10.5194/acp-21-6389-2021, 2021.

716 Pinder, R. W., Adams, P. J. and Pandis, S. N.: Ammonia Emission Controls as a Cost-Effective Strategy for
717 Reducing Atmospheric Particulate Matter in the Eastern United States, Environ. Sci. Technol., 41(2), 380–386,
718 doi:10.1021/es060379a, 2007.

719 Pinder, R. W., Gilliland, A. B. and Dennis, R. L.: Environmental impact of atmospheric NH3 emissions under
720 present and future conditions in the eastern United States, Geophys. Res. Lett., 35(12),
721 doi:10.1029/2008GL033732, 2008.

722 Pollution, C. and Board, C.: Guidelines for Manual Sampling & Analyses., 2011.

723 Saraswati, George, M. P., Sharma, S. K., Mandal, T. K. and Kotnala, R. K.: Simultaneous Measurements of
724 Ambient NH 3 and Its Relationship with Other Trace Gases, PM 2.5 and Meteorological Parameters over Delhi,
725 India, Mapan - J. Metrol. Soc. India, 34(1), 55–69, doi:10.1007/s12647-018-0286-0, 2019.

726 Seinfeld, J. H. and Pandis, S. N.: Atmospheric chemistry and physics : from air pollution to climate change., n.d.

727 Seinfeld, J. H., Bretherton, C., Carslaw, K. S., Coe, H., DeMott, P. J., Dunlea, E. J., Feingold, G., Ghan, S.,
728 Guenther, A. B., Kahn, R., Kraucunas, I., Kreidenweis, S. M., Molina, M. J., Nenes, A., Penner, J. E., Prather, K.
729 A., Ramanathan, V., Ramaswamy, V., Rasch, P. J., Ravishankara, A. R., Rosenfeld, D., Stephens, G. and Wood,
730 R.: Improving our fundamental understanding of the role of aerosol–cloud interactions in the climate system, Proc.
731 Natl. Acad. Sci. U. S. A., 113(21), 5781, 2016.

732 Sha, T., Ma, X., Jia, H., Tian, R., Chang, Y., Cao, F. and Zhang, Y.: Aerosol chemical component: Simulations

733 with WRF-Chem and comparison with observations in Nanjing, Atmos. Environ., 218(June), 116982,

734 doi:10.1016/j.atmosenv.2019.116982, 2019.

735 Sharma, C., Tiwari, M. K. and Pathak, H.: Estimates of emission and deposition of reactive nitrogenous species

736 for India, Curr. Sci., 94(11), 1439–1446, 2008.

737 Sharma, G., Sinha, B., Pallavi, Hakkim, H., Chandra, B. P., Kumar, A. and Sinha, V.: Gridded Emissions of CO,

738 NOx, SO2, CO2, NH3, HCl, CH4, PM2.5, PM10, BC, and NMVOC from Open Municipal Waste Burning in

739 India, Environ. Sci. Technol., 53(9), 4765–4774, doi:10.1021/acs.est.8b07076, 2019.

740 Sharma, S. K., Saxena, M., Saud, T., Korpole, S. and Mandal, T. K.: Measurement of NH3, NO, NO2 and related

741 particulates at urban sites of indo gangetic plain (IGP) of India, J. Sci. Ind. Res. (India)., 71(5), 360–362, 2012.

742 Sharma, S. K., Harit, R. C., Kumar, V., Mandal, T. K. and Pathak, H.: Ammonia Emission from Rice-Wheat

743 Cropping System in Subtropical Soil of India, Agric. Res., 3(2), 175–180, doi:10.1007/s40003-014-0107-9,

744 2014a.

745 Sharma, S. K., Kumar, M., Rohtash, Gupta, N. C., Saraswati, Saxena, M. and Mandal, T. K.: Characteristics of

746 ambient ammonia over Delhi, India., 2014b.

747 Sharma, S. K., Kotnala, G. and Mandal, T. K.: Spatial Variability and Sources of Atmospheric Ammonia in India:

748 A Review, Aerosol Sci. Eng., 4(1), doi:10.1007/s41810-019-00052-3, 2020.

749 Sherlock, R. R., Freney, J. R., Bacon, P. E. and van der Weerden, T. J.: Estimating ammonia volatilization from

750 unsaturated urea fertilized and urine affected soils by an indirect method, Fertil. Res., 40(3), 197–205,

751 doi:10.1007/BF00750466, 1994.

752 Singh, G. K., Rajeev, P., Paul, D. and Gupta, T.: Chemical characterization and stable nitrogen isotope

753 composition of nitrogenous component of ambient aerosols from Kanpur in the Indo-Gangetic Plains., Sci. Total

754 Environ., 763, 143032, doi:10.1016/j.scitotenv.2020.143032, 2021.

755 Stieger, B., Spindler, G., van Pinxteren, D., Grüner, A., Wallasch, M. and Herrmann, H.: Development of an

756 online-coupled MARGA upgrade for the 2\,h interval quantification of low-molecular-weight organic acids in the

757 gas and particle phases, Atmos. Meas. Tech., 12(1), 281–298, doi:10.5194/amt-12-281-2019, 2019.

758 Sutton, M. A. and Howard, C. M.: Ammonia maps make history, Nature, 564(7734), 49–50, 2018.

759 Sutton, M. A., Burkhardt, J. K., Guerin, D., Nemitz, E. and Fowler, D.: Development of resistance models to

760 describe measurements of bi-directional ammonia surface-atmosphere exchange, Atmos. Environ., 32(3), 473–

761 480, doi:10.1016/S1352-2310(97)00164-7, 1998.

762 Sutton, M. A., Erisman, J. W., Dentener, F. and Möller, D.: Ammonia in the environment: From ancient times to

763 the present, Environ. Pollut., 156(3), 583–604, doi:10.1016/j.envpol.2008.03.013, 2008.

764 Sutton, M. A., Reis, S. and Baker, S. M. H.: Atmospheric Ammonia: Detecting emission changes and

765 environmental impacts., 2009a.

766 Sutton, M. A., Nemitz, E., Milford, C., Campbell, C., Erisman, J. W., Hensen, A., Cellier, P., David, M., Loubet,

767 B., Personne, E., Schjoerring, J. K., Mattsson, M., Dorsey, J. R., Gallagher, M. W., Horvath, L., Weidinger, T.,

768 Meszaros, R., Dämmgen, U., Neftel, A., Herrmann, B., Lehman, B. E., Flechard, C. and Burkhardt, J.: Dynamics

769 of ammonia exchange with cut grassland: synthesis of results and conclusions of the GRAMINAE Integrated

770 Experiment, Biogeosciences, 6(12), 2907–2934, doi:10.5194/bg-6-2907-2009, 2009b.

771 Sutton, M. A., Reis, S., Riddick, S. N., Dragosits, U., Nemitz, E., Theobald, M. R., Tang, Y. S., Braban, C. F.,

772   Vieno, M., Dore, A. J., Mitchell, R. F., Wanless, S., Daunt, F., Fowler, D., Blackall, T. D., Milford, C., Flechard,

773   C. R., Loubet, B., Massad, R., Cellier, P., Personne, E., Coheur, P. F., Clarisse, L., Van Damme, M., Ngadi, Y.,

774   Clerbaux, C., Skjøth, C. A., Geels, C., Hertel, O., Kruit, R. J. W., Pinder, R. W., Bash, J. O., Walker, J. T.,

775   Simpson, D., Horváth, L., Misselbrook, T. H., Bleeker, A., Dentener, F. and de Vries, W.: Towards a climate-

776   dependent paradigm of ammonia emission and deposition, Philos. Trans. R. Soc. B Biol. Sci., 368(1621),

777   20130166–20130166, doi:10.1098/rstb.2013.0166, 2013.

778   Sutton, M. A., Drewer, J., Moring, A., Adhya, T. K., Ahmed, A., Bhatia, A., Brownlie, W., Dragosits, U., Ghude,

779   S. D., Hillier, J., Hooda, S., Howard, C. M., Jain, N., Kumar, D., Kumar, R. M., Nayak, D. R., Neeraja, C. N.,

780   Prasanna, R., Price, A., Ramakrishnan, B., Reay, D. S., Singh, R., Skiba, U., Smith, J. U., Sohi, S., Subrahmanyan,

781   D., Surekha, K., van Grinsven, H. J. M., Vieno, M., Voleti, S. R., Pathak, H. and Raghuram, N.: 2 - The Indian

782   Nitrogen Challenge in a Global Perspective, in The Indian Nitrogen Assessment, edited by Y. P. Abrol, T. K.

783   Adhya, V. P. Aneja, N. Raghuram, H. Pathak, U. Kulshrestha, C. Sharma, and B. Singh, pp. 9–28, Elsevier.,

784   2017a.

785   Sutton, M. A., J. Drewer, A. Moring, T.K Adhya, A. Ahmed and A. Bhatia: The Indian nitrogen assessment :

786   sources of reactive nitrogen, environmental and climate effects, management options, and policies, in The Indian

787   Nitrogen Assessment, edited by Y. P. Abrol, T. K. Adhya, V. P. Aneja, N. Raghuram, H. Pathak, U. Kulshrestha,

788   C. Sharma, and B. Singh, pp. 9–25, Elsevier., 2017b.

789   Sutton, M. A., Van Dijk, N., Levy, P. E., Jones, M. R., Leith, I. D., Sheppard, L. J., Leeson, S., Sim Tang, Y.,

790   Stephens, A., Braban, C. F., Dragosits, U., Howard, C. M., Vieno, M., Fowler, D., Corbett, P., Naikoo, M. I.,

791   Munzi, S., Ellis, C. J., Chatterjee, S., Steadman, C. E., Móring, A. and Wolseley, P. A.: Alkaline air: changing

792   perspectives on nitrogen and air pollution in an ammonia-rich world: Alkaline Air, Philos. Trans. R. Soc. A Math.

793   Phys. Eng. Sci., 378(2183), doi:10.1098/rsta.2019.0315, 2020.

794   Technical specifications for CAAQM station: TECHNICAL SPECIFICATIONS FOR CONTINUOUS

795   AMBIENT AIR QUALITY MONITORING (CAAQM) STATION (REAL TIME) Central Pollution Control

796   Board East Arjun Nagar , Shahdara., 2019.

797   Thomas, R. M., Trebs, I., Otjes, R., Jongejan, P. A. C., Brink, H. ten, Phillips, G., Kortner, M., Meixner, F. X.

798   and Nemitz, E.: An Automated Analyzer to Measure Surface-Atmosphere Exchange Fluxes of Water Soluble

799   Inorganic Aerosol Compounds and Reactive Trace Gases, Environ. Sci. \& Technol., 43(5), 1412–1418,

800   doi:10.1021/es8019403, 2009.

801   Twigg, M. M., Di Marco, C. F., Leeson, S., van Dijk, N., Jones, M. R., Leith, I. D., Morrison, E., Coyle, M.,

802   Proost, R., Peeters, A. N. M., Lemon, E., Frelink, T., Braban, C. F., Nemitz, E. and Cape, J. N.: Water soluble

803   aerosols and gases at a UK background site – Part 1: Controls of $PM_{2.5}$ and PM_{10} aerosol

804   composition, Atmos. Chem. Phys., 15(14), 8131–8145, doi:10.5194/acp-15-8131-2015, 2015.

805   Wagh, S., Singh, P., Ghude, S. D., Safai, P., Prabhakaran, T. and Kumar, P. P.: Study of ice nucleating particles

806   in fog-haze weather at New Delhi, India: A case of polluted environment, Atmos. Res., 259, 105693,

807   doi:https://doi.org/10.1016/j.atmosres.2021.105693, 2021.

808   Wang, Q., Miao, Y. and Wang, L.: Regional transport increases ammonia concentration in Beijing, China,

809   Atmosphere (Basel)., 11(6), doi:10.3390/ATMOS11060563, 2020a.

810   Wang, S., Nan, J., Shi, C., Fu, Q., Gao, S., Wang, D., Cui, H., Saiz-Lopez, A. and Zhou, B.: Atmospheric ammonia

811   and its impacts on regional air quality over the megacity of Shanghai, China, Sci. Rep., 5(October), 1–13,

812   doi:10.1038/srep15842, 2015.

813   Wang, T., Song, Y., Xu, Z., Liu, M., Xu, T., Liao, W., Yin, L., Cai, X., Kang, L., Zhang, H. and Zhu, T.: Why is

814   the Indo-Gangetic Plain the region with the largest NH3column in the globe during pre-monsoon and monsoon

815   seasons?, Atmos. Chem. Phys., 20(14), 8727–8736, doi:10.5194/acp-20-8727-2020, 2020b.

816   Warner, J. X., Dickerson, R. R., Wei, Z., Strow, L. L., Wang, Y. and Liang, Q.: Increased atmospheric ammonia

817   over the world's major agricultural areas detected from space, Geophys. Res. Lett., 44(6), 2875–2884,

818   doi:10.1002/2016GL072305, 2017.

819   Wentworth, G. R., Murphy, J. G., Gregoire, P. K., Cheyne, C. A. L., Tevlin, A. G. and Hems, R.: Soil-atmosphere

820   exchange of ammonia in a non-fertilized grassland: Measured emission potentials and inferred fluxes,

821   Biogeosciences, 11(20), 5675–5686, doi:10.5194/bg-11-5675-2014, 2014.

822   Wentworth, G. R., Murphy, J. G., Benedict, K. B., Bangs, E. J. and Collett, J. L.: The role of dew as a night-time

823   reservoir and morning source for atmospheric ammonia, Atmos. Chem. Phys., 16(11), 7435–7449,

824   doi:10.5194/acp-16-7435-2016, 2016.

825   Xu, J., Chen, J., Huo, J., Lin, Y., Fu, Q., Guo, H. and Lee, S. H.: Importance of gas-particle partitioning of

826   ammonia in haze formation in the rural agricultural environment, Atmos. Chem. Phys., 20(12), 7259–7269,

827   doi:10.5194/acp-20-7259-2020, 2020.

828   Yang, J., Kang, S. and Ji, Z.: Sensitivity analysis of chemical mechanisms in the WRF-chem model in

829   reconstructing aerosol concentrations and optical properties in the Tibetan Plateau, Aerosol Air Qual. Res., 18(2),

830   505–521, doi:10.4209/aaqr.2017.05.0156, 2018.

831   Zhang, X., Liu, J., Han, H., Zhang, Y., Jiang, Z., Wang, H., Meng, L., Li, Y. C. and Liu, Y.: Satellite-Observed

832   Variations and Trends in Carbon Monoxide over Asia and Their Sensitivities to Biomass Burning, Remote Sens.,

833   12(5), 830, doi:10.3390/rs12050830, 2020.

834

835

836

837

838

839

840

841

842

843

844

845

846

847

FIGURE CAPTIONS

Figure 1. (a) Comparison of observed and simulated average diurnal variation in (a) meteorological parameters such as Temperature (T in °c) and Relative humidity (RH in %) and (b) NH_3 and NH_4^+ concentration ($\mu g\ m^{-3}$) during the sampling period (bar indicates mean standard deviation of each hour).

Figure 2. Ratio of model/obs of the daily mean NH_3, NH_4^+ and total NH_x concentration

Figure 3. Share of major components of gases and particulate matter ($PM_{2.5}$) based on the mean concentrations during WiFEX (share according to $\mu eq\ m^{-3}$).

Figure 4. Fraction of HCl/Cl^- ratio as a function of NH_4^+ concentration ($\mu g\ m^{-3}$) and Relative humidity (RH)

Figure 5. Bivariate plots of mean (a) NH_3 concentration (b) NH_4^+ concentration (c) Cl^- concentration and (d) total NH_x concentration in relation to wind speed ($m\ s^{-1}$) and direction.

Figure 6. Neutralizing effect between Cl^-, NO_3^- and SO_4^{2-} as the anions ($\mu eq\ m^{-3}$) and aerosol neutralization ratio (ANR) where, ANR>1 indicates over neutralized (alkaline) and ANR<1 indicates under neutralized (acid) (orange bar indicates daily mean standard error).

Figure 7. Box-Whiskers plot for trace gases and secondary inorganic aerosols from the observations (MARGA) and simulated in sensitivity test with changes in HCl emissions (No HCl (0 mol $km^{-2}\ h^{-1}$), Base Case HCl (24.8 mol $km^{-2}\ h^{-1}$), and 3×Base HCl (74 mol $km^{-2}\ h^{-1}$)) at IGIA, Delhi.

Figure 8. (top) Average diurnal cycles of NH_3 and NH_4^+ concentration ($\mu g\ m^{-3}$) with mole equivalents of Cl^-, NO_3^-, SO_4^{2-}, NH_4^+, SO_2, HCl and HNO_3 ($\mu eq\ m^{-3}$) of (a) measured (MARGA) and (b) modeled (3×Base HCl run) along with its meteorological parameters (bottom).

Figure 9. Diurnal variation in the mean (a) NH_3 concentration (b) NH_4^+ concentration and (c) total NH_x concentration observed (black), simulated in No HCl (red dotted), Base Case HCl (red dash) and 3×Base HCl run (red solid).

Figure 10. Comparison of ratio of model/obs in the daily mean (a) NH_3 concentration (b) NH_4^+ concentration and (c) total NH_x concentration in 3×Base HCl and -3×NH_3_EMI scenario.

888   **TABLES**

889   **Table 1. Performance statistics of correlation coefficient (r) of NH_4^+/NH_x with NH_3 and aerosols (NH_4^+, Cl^-**

890   **, SO_4^{2-}, and NO_3^-)**

891

Gases and Aerosols	MARGA Correlation coefficient (r) with NH_4^+/NH_x ratio	Model Correlation coefficient (r) with NH_4^+/NH_x ratio
Ammonia (NH_3)	-0.57	-0.58
Ammonium (NH_4^+)	0.70	0.67
Chloride (Cl^-)	0.79	-
Sulfate (SO_4^-)	0.09	0.77
Nitrate (NO_3^-)	0.13	0.57

892
893
894
895
896
897
898
899
900
901
902
903
904
905
906
907
908
909
910
911
912
913
914
915
916

Table 2. Daily mean $\pm$ 1σ in gases and inorganic aerosol concentration observed (MARGA) and simulated in sensitivity test with changes in total HCl emissions (No HCl (0 mol km^{-2} h^{-1}), Base Case HCl (24.8 mol km^{-2} h^{-1}), and 3×Base HCl (74 mol km^{-2} h^{-1}).

Species concentration (μg m^{-3})	MARGA	No HCl	Base Case HCl	3×Base HCl
NH_3	20 ± 8.52	50.2 ± 11.7	48.2 ± 11.31	44.5 ± 10.8
NH_4^+	35.9 ± 17.7	13.9 ± 3.04	21.4 ± 6.65	34.5 ± 15.2
NH_x	56.6 ± 17.1	64 ± 13.2	69.6 ± 16.6	79.5 ± 23.7
Cl^-	50.6 ± 39.4	-	15.1 ± 9.65	40.9 ± 27.2
NO_3^-	27.9 ± 8.17	35.9 ± 7.23	35.6 ± 7.05	35.5 ± 7.03
SO_4^{2-}	17.1 ± 5.63	9.62 ± 2.78	9.56 ± 2.71	9.56 ± 2.71
HCl	0.86 ± 0.35	-	0.20 ± 0.23	0.22 ± 0.25
HNO_3	3.43 ± 1.68	0.18 ± 0.21	0.17 ± 0.22	0.18 ± 0.23
SO_2	30.6 ± 18.4	46.6 ± 12.4	46.7 ± 12.4	46.7 ± 12.4

Table 3. Model performance statistics for NH_3, NH_4^+ and total NH_x concentration at IGIA, Delhi from three sensitivity experiments (No HCl (0 mol km^{-2} h^{-1}), Base Case HCl (24.8 mol km^{-2} h^{-1}), and 3×Base HCl (74 mol km^{-2} h^{-1})) and the MARGA

Species	No HCl		Base Case HCl		3×Base HCl	
	Correlation coefficient (*r*)	Normalised Mean Bias (NMB)	Correlation coefficient (*r*)	Normalised Mean Bias (NMB)	Correlation coefficient (*r*)	Normalised Mean Bias (NMB)
NH_3	-0.58	1.38	-0.60	1.29	-0.65	1.13
NH_4^+	0.45	-0.61	0.75	-0.40	0.76	-0.03
NH_x	0.69	0.12	0.70	0.22	0.70	0.39

956   **Figure 1**
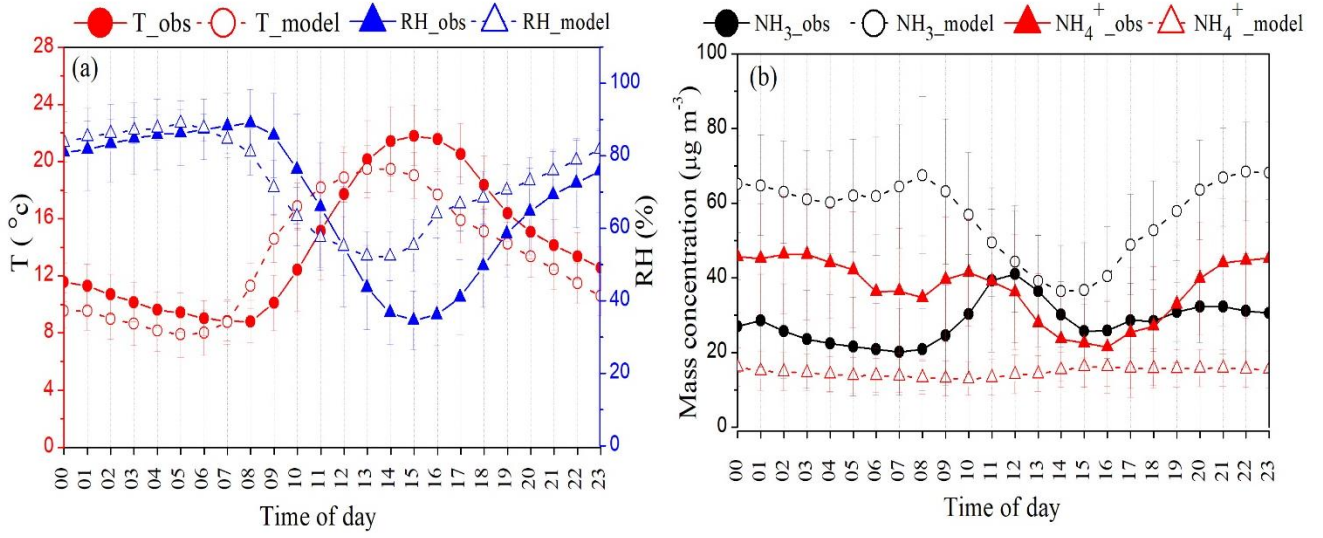
957
958

959   **Figure 2**
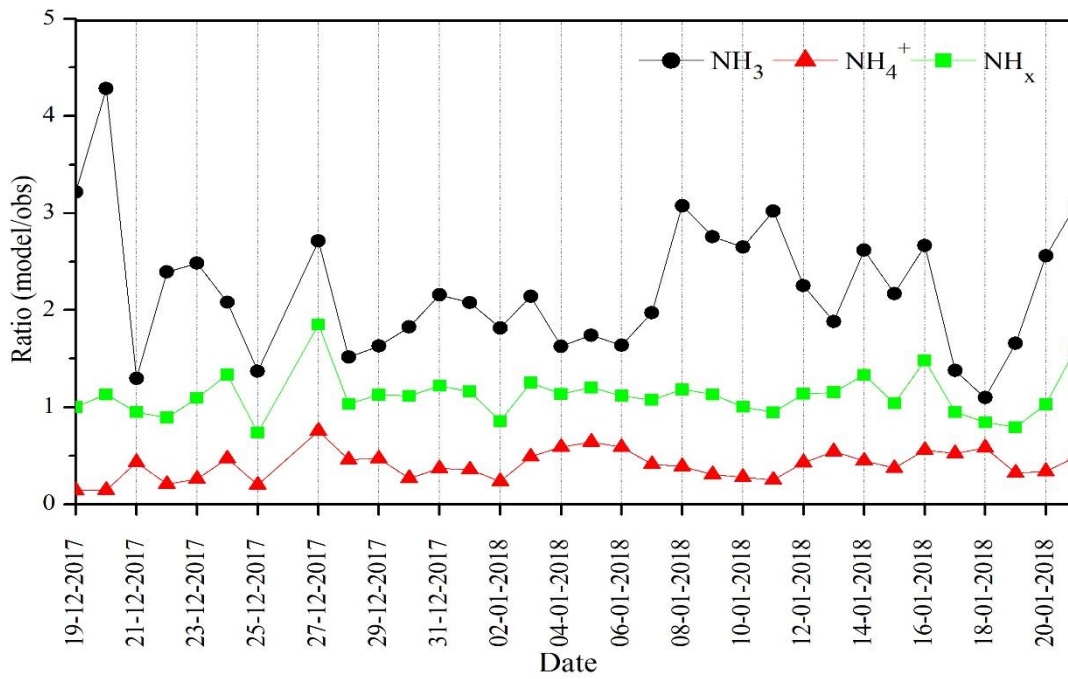
960
961
962
963

964 **Figure 3**
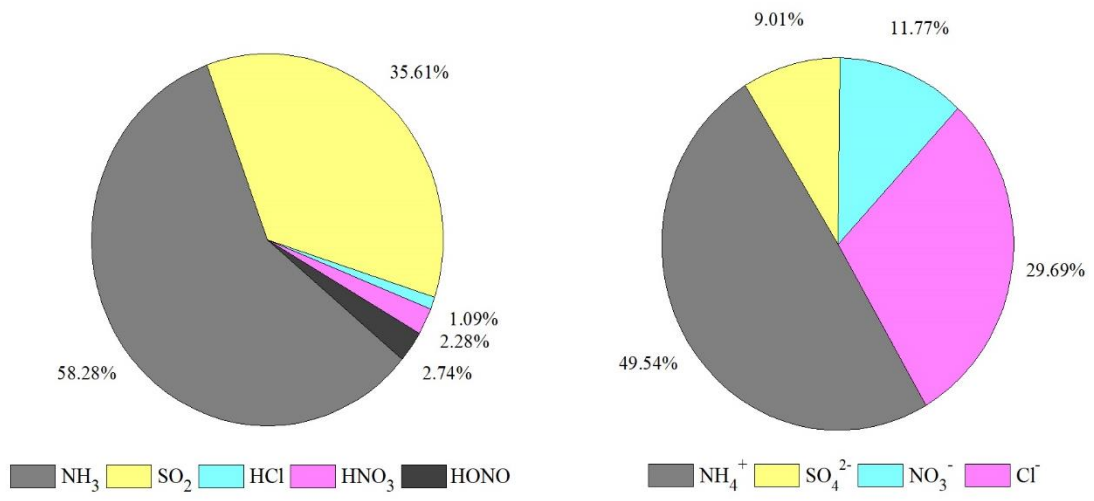
965

966

967

968 **Figure 4**
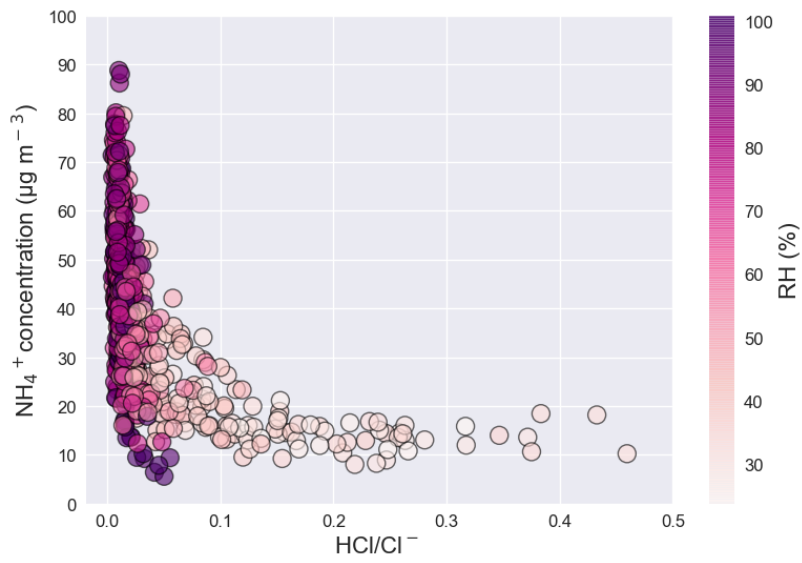
969

970

971

972

973 **Figure 5**
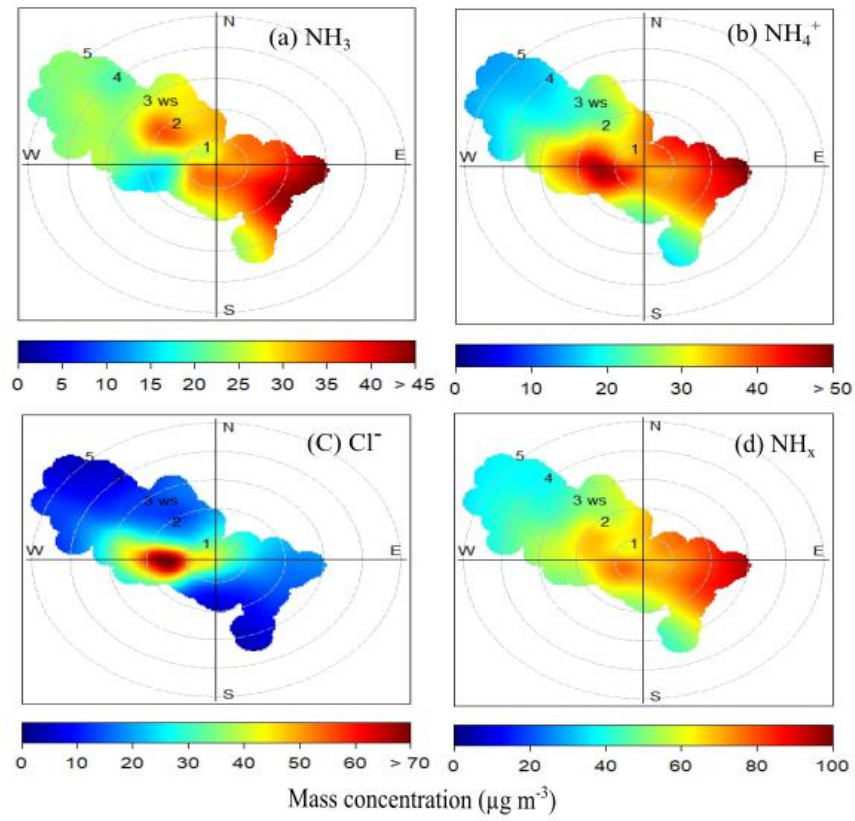
974

975 **Figure 6**
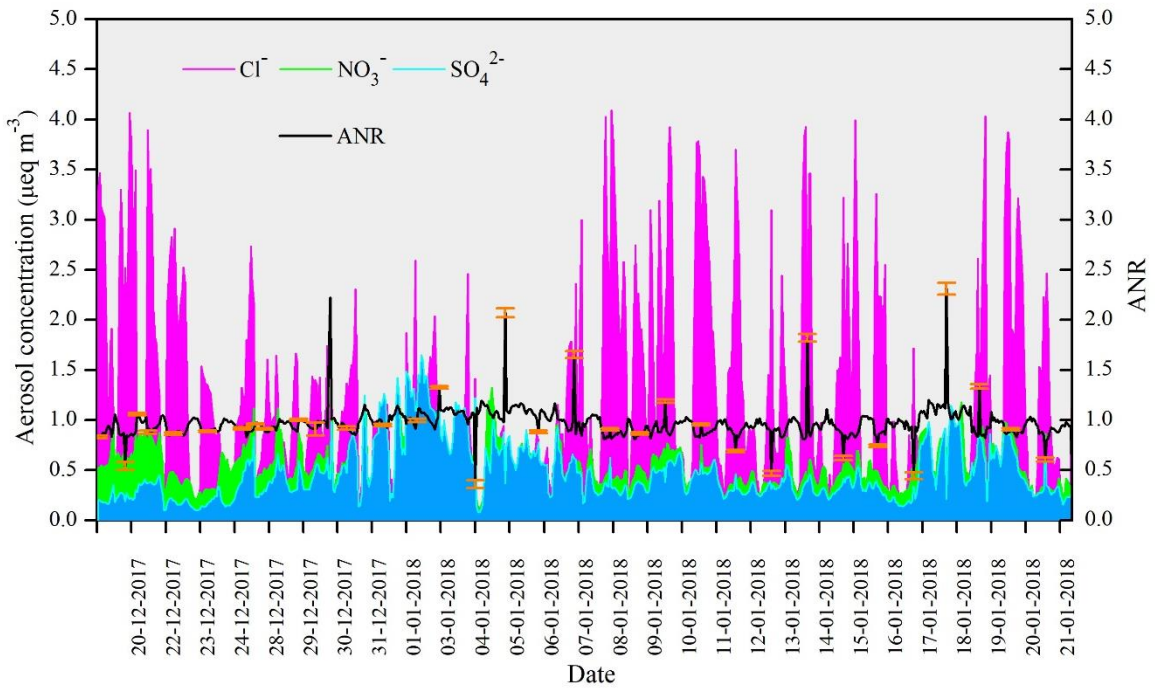
976
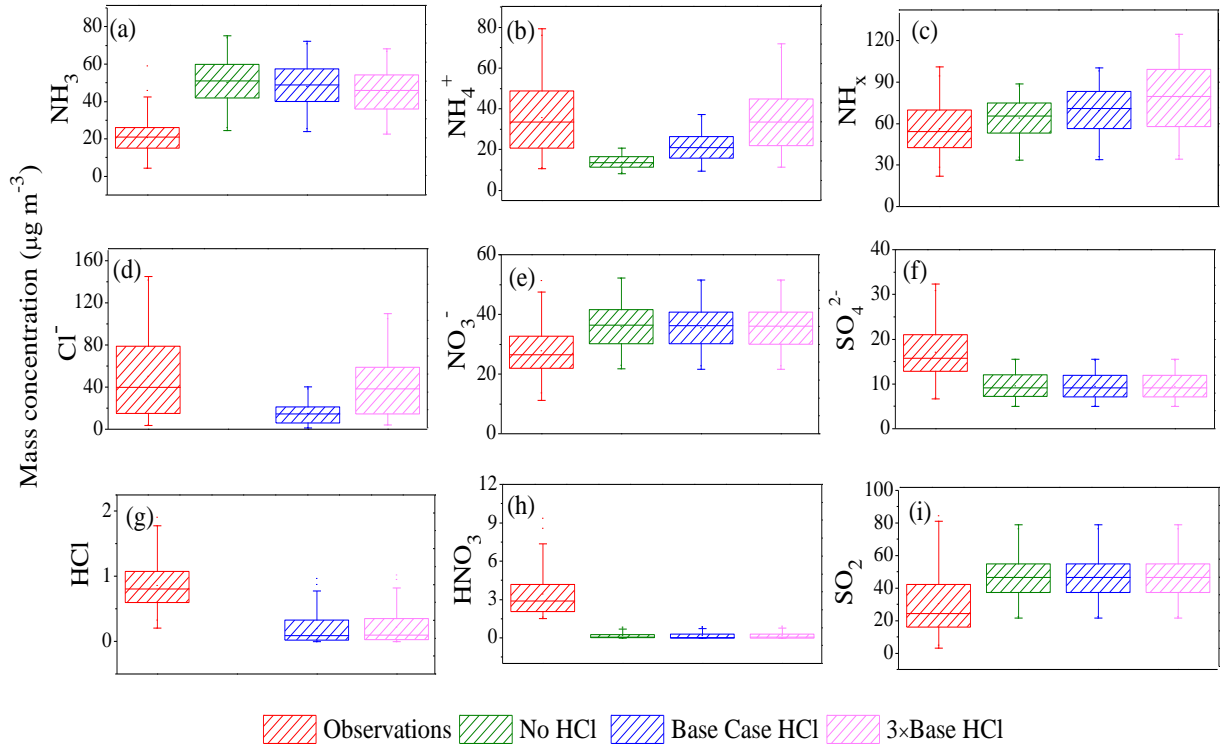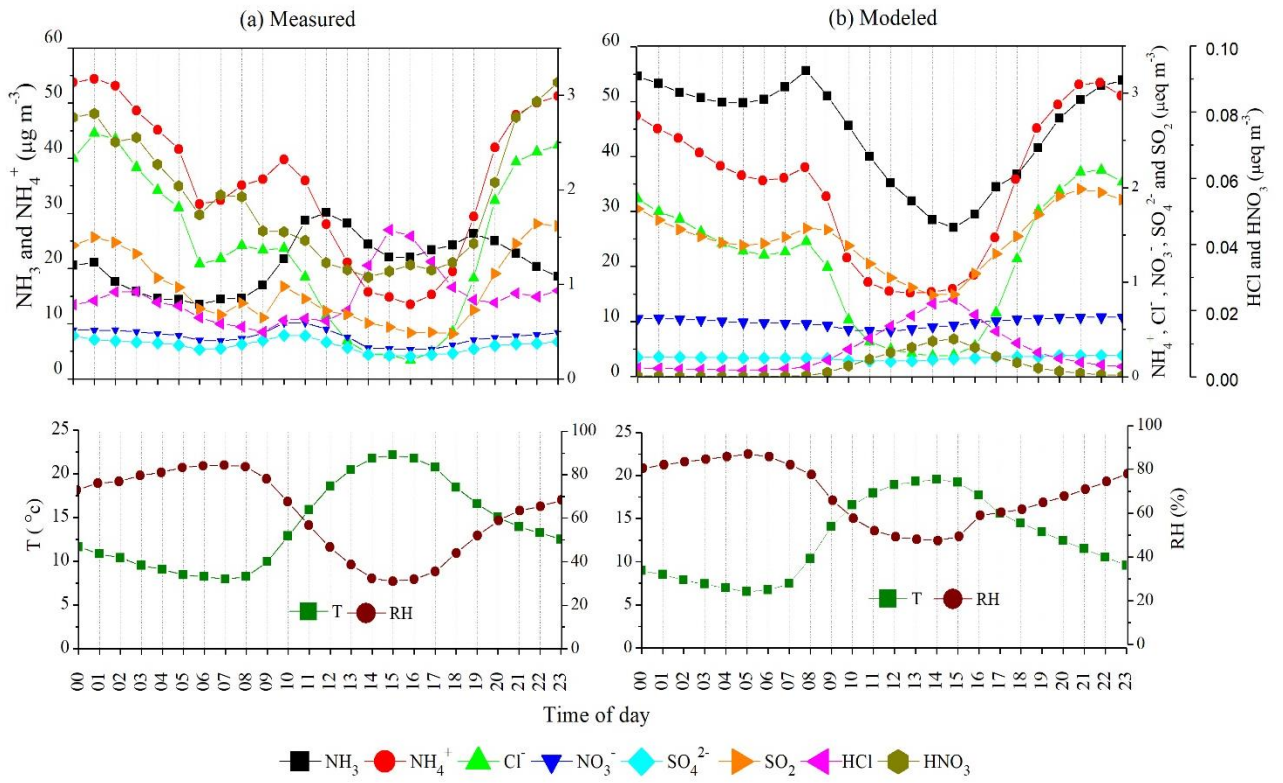
Figure 7

997   **Figure 8**

1017   **Figure 9**
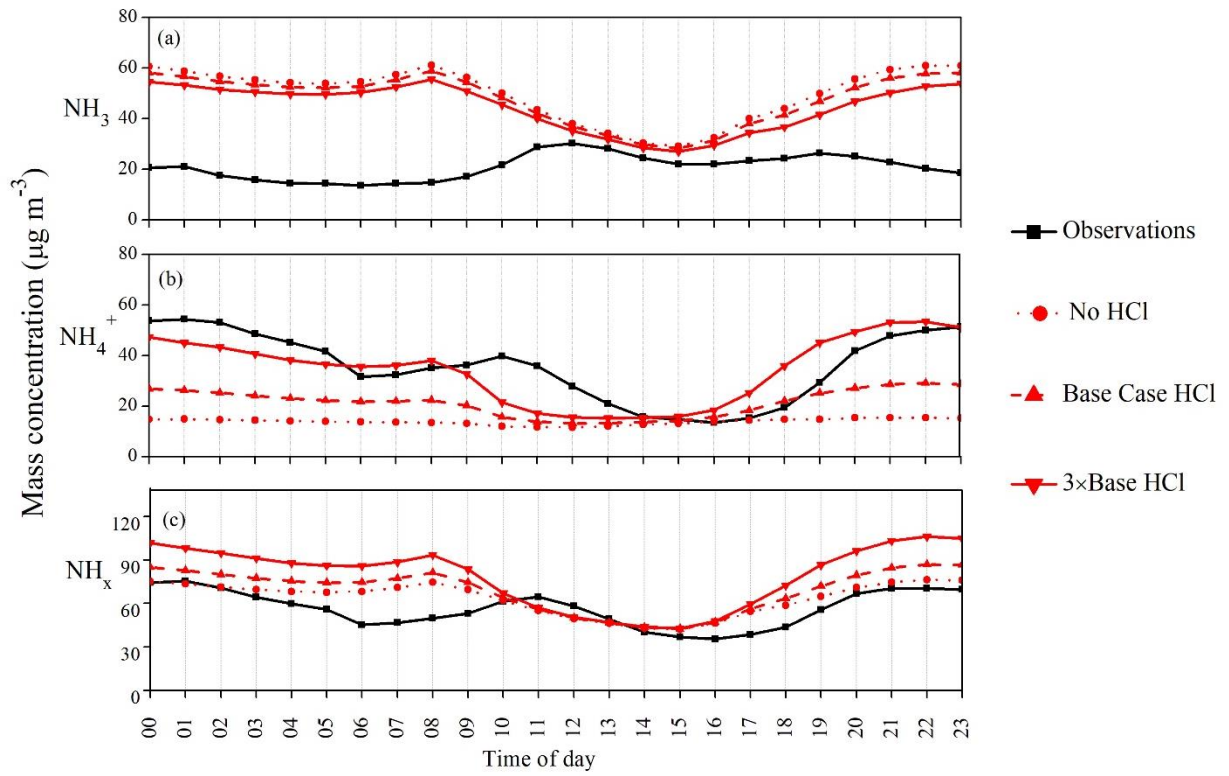
1034   **Figure 10**
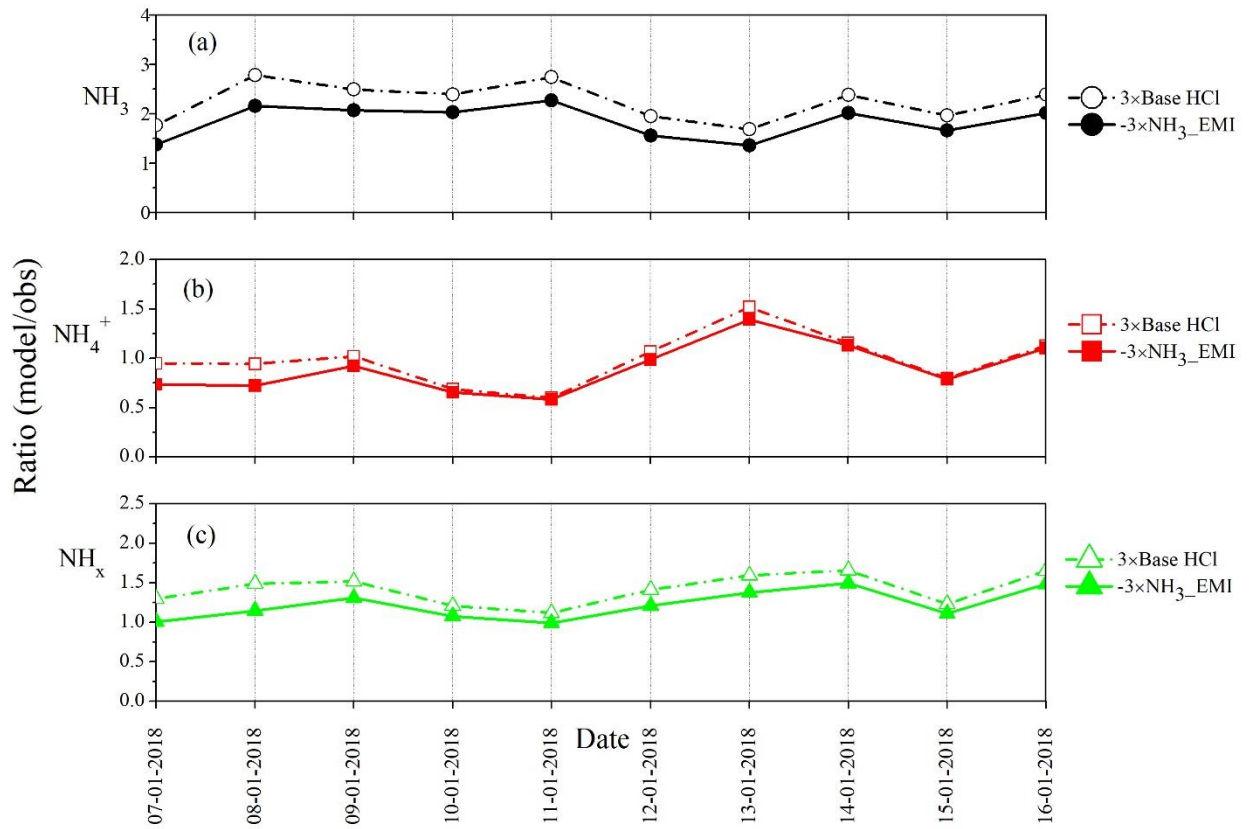
1035
1036
1037
1038
1039
1040
1041
1042
1043